JCIM JOURNAL OF CHEMICAL INFORMATION AND MODELING

Article

Cite This: J. Chem. Inf. Model. 2018, 58, 383−404

pubs.acs.org/jcim

Allosteric Modulation of Human Hsp90α Conformational Dynamics

David L. Penkler,[†] Canan Atilgan,[‡] and Özlem Tastan Bishop*[,†]

[†]Research Unit in Bioinformatics (RUBi), Department of Biochemistry and Microbiology, Rhodes University, Grahamstown, 6140, South Africa

[‡]Faculty of Engineering and Natural Sciences, Sabanci University, Tuzla 34956, Istanbul, Turkey

Supporting Information

ABSTRACT: Central to Hsp90's biological function is its ability to interconvert between various conformational states. Drug targeting of Hsp90's regulatory mechanisms, including its modulation by cochaperone association, presents as an attractive therapeutic strategy for Hsp90 associated pathologies. In this study, we utilized homology modeling techniques to calculate full-length structures of human Hsp90α in closed and partially open conformations and used these structures as a basis for several molecular dynamics based analyses aimed at elucidating allosteric mechanisms and modulation sites in human Hsp90α. Atomistic simulations demonstrated that bound adenosine triphosphate (ATP) stabilizes the dimer by "tensing" each protomer, while adenosine diphosphate (ADP) and apo configurations "relax" the complex by increasing global flexibility, the former case resulting in a fully open "v-like" conformation. Dynamic residue network analysis revealed regions of the protein involved in intraprotein communication and identified several key communication hubs that correlate with known functional sites. Pairwise comparison of betweenness centrality, shortest path, and residue fluctuations revealed that a proportional relationship exists between the latter two measurables and an inverse relationship between these two and betweenness centrality. This analysis showed how protein flexibility, degree of compactness, and the distance cutoff used for network construction influence the correlations between these metrics. These findings are novel and suggest shortest path and betweenness centrality to be more relevant quantities to follow for detecting functional residues in proteins compared to residue fluctuations. Perturbation response scanning analysis identified several potential residue sites capable of modulating conformational change in favor of interstate conversion. For the ATP-bound open conformation, these sites were found to overlap with known Aha1 and client binding sites, demonstrating how naturally occurring forces associated with cofactor binding could allosterically modulate conformational dynamics.

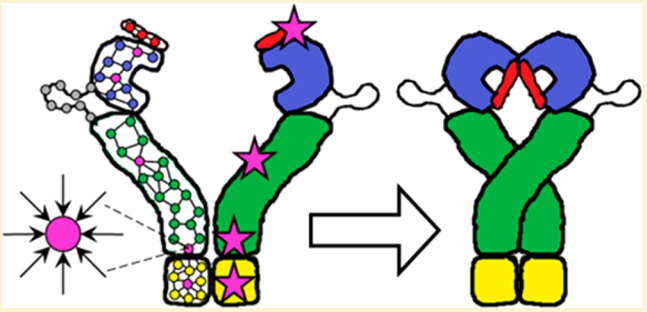

INTRODUCTION

The 90 kDa heat shock protein (Hsp90) is a highly conserved molecular chaperone that plays a central role in maintaining cellular homeostasis in organisms of all kingdoms of life with the exception of the archea.[1] Hsp90's biological function is centered around its ability to facilitate the folding, maturation, and trafficking of a wide array of client peptides.[2−4] The related functions of these clients implicate Hsp90 with numerous cellular functions, ranging from signal transduction to complex regulatory mechanisms, as well as innate and adaptive immunity.[5] Hsp90 is thus uniquely positioned at the crossroads of several fundamental cellular pathways, representing a central hub in protein interaction networks.[1] Also included in Hsp90's broad client base are known disease related peptides, association of which implicate the chaperone in the progression of several pathologies including various protein misfolding disorders, cancer, and neurological diseases.[6] Indeed, it has become increasingly clear that deregulation of Hsp90 may present an attractive strategy for disease treatment, leading to a growing interest in Hsp90 as a viable drug target particularly in the field of molecular oncology[7−9] and parasitology.[10−12]

Biochemical and structural studies have revealed that Hsp90 exists as a homodimer, and that each protomer is characterized by three well-defined domains:[6,13,14] the N-terminal domain (NTD) is responsible for adenosine triphosphate (ATP) binding and hydrolysis as well as facilitating protomer dimerization,[15] the middle domain (M-domain) contributes to ATPase activation[16] and provides a large surface area suitable for Hsp90's broad range of client protein interactions, and the C-terminal domain (CTD) provides the primary interprotomer dimerization site.[17,18] The NTD and M-domain are connected via a highly flexible charged linker that is thought to be involved in modulating chaperone function.[19−22]

Hsp90's ability to bind and release client proteins revolves around a complex nucleotide dependent conformational cycle in which the dimer transitions between a catalytically inactive open state and an active closed state (Figure 1). Crystal structures of the *Escherichia coli* Hsp90 homologue, HtpG, revealed that in the nucleotide free state, dimerization occurs at

Received: October 26, 2017
Published: January 29, 2018

DOI: 10.1021/acs.jcim.7b00630
J. Chem. Inf. Model. 2018, 58, 383−404

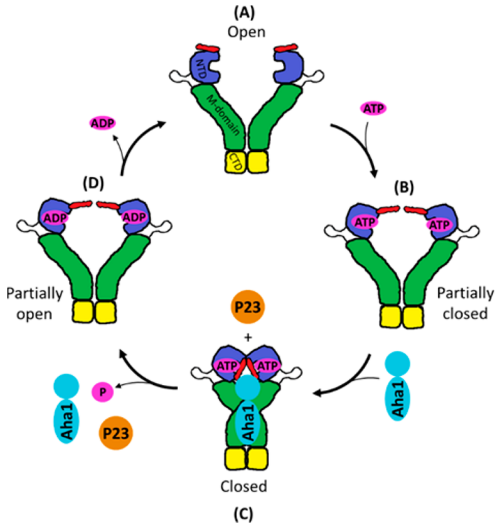

Figure 1. Hsp90's nucleotide dependent conformational cycle: (A) nucleotide free open conformation; (B) ATP binding induces NTD restructuring and the slow closure of the ATP-lid; (C) interactions with the cochaperone Aha1 accelerates ATP-lid closure and promotes NTD dimerization, completing the conformational transition toward the closed state; (D) ATP hydrolysis and subsequent binding of ADP triggers protomer uncoupling and a transition toward the open conformation. Release of ADP returns the dimer to its original state. Domains are colored as follows: NTD (blue); M-domain (green); and CTD (yellow). The ATP-lid is shown in red.

the CTD alone and Hsp90 adopts an open "v-like" conformation in which the M-domains are suitably exposed in preparation for client loading[23−25] (Figure 1A). Binding of ATP triggers conformational rearrangements that lead to NTD dimerization and an eventual conformational transition toward the closed catalytically active state. Central to this conformational switch is the behavior of the ATP-lid which must close over the nucleotide binding pocket to entrap the bound nucleotide and, in doing so, exposes essential hydrophobic surfaces which facilitate NTD dimerization (Figure 1B).[17,26] Transition to the closed state and full ATPase activation is an inherently slow process, recording time constants in the order of minutes.[15,27,28] The transition is likely to occur via structural intermediates, which may present further energy barriers that must be overcome.[29,30] Crystal structures of mammalian Hsp90, Grp94, have revealed structurally identical partially open/closed putative intermediate conformations of Hsp90 when bound by either adenosine diphosphate (ADP) or nonhydrolyzable ATP[24] (Figure 1B and D). In addition to nucleotide regulation, cochaperone interactions have been shown to play an important role in the modulation of Hsp90's ATPase activity.[26,31] Interaction with the cochaperone Aha1 has been shown to increase ATPase activity 10-fold, by promoting the closing transition through the facilitation of ATP-lid closure[30] and structurally reorienting an essential M-domain catalytic loop toward the ATPase site, where it is required to coordinate with the γ-phosphate of ATP.[16] Hsp90's catalytically active conformation (Figure 1C) has been well described through crystal structures of yeast Hsp90[17] and human Hsp90$_\beta$.[32] Both structures were crystallized in complex with ATP and demonstrate structurally similar closed conformations in which the protomers are partially twisted around one another, with fully closed ATP-lids, and projection of the catalytic loops into the nucleotide binding pockets. This closed conformation is thought to be stabilized by NTD interactions with the cochaperone p23/sba1[17] (Figure 1C). Eventual ATP hydrolysis and the subsequent binding of ADP triggers a conformational shift back to the open state. Under these conditions, Aha1 and p23/sba1 are released permitting protomer uncoupling at the NTD. The subsequent repositioning of the ATP-lid back to its open conformation (Figure 1D) allows for ADP release, completing the conformational switch back to the nucleotide free open conformation (Figure 1A).

To date, a number of computational studies, aimed at elucidating the mechanistic regulation of Hsp90's conformational dynamics, have been carried out based largely on the available experimental structural data. Atomic resolution models of allosteric regulation in Hsp90 have been proposed, in which reported cross-talk between the NTD and CTD implicated ATP binding and hydrolysis at the NTD to have a strong influence on conformational dynamics at the CTD.[33,34] These studies lead to the prediction of allosteric inhibitor ligands that bind an allosteric target site identified in the CTD.[35−37] Coarse grained and atomistic approaches coupled with energy landscape analysis were used to demonstrate the global motions and functional dynamics of Hsp90, reporting a network of conserved regions within the protein that may be important for regulating intraprotomer communications in response to ATP hydrolysis.[38] A comprehensive all atom simulation study of several Hsp90 crystal structures from different organisms demonstrated how the functional dynamics of Hsp90 are modulated by the motion of quasi-rigid domains involving two sets of conserved residues that form interdomain hinges between the NTD/M-domain and M-domain/CTD.[39] Atomistic simulations coupled with force distribution analysis of the HtpG structure revealed allosteric communication pathways connecting a similar M-domain hinge and putative client binding site with the NTD nucleotide binding site.[40] Thermodynamic analyses of molecular dynamics (MD) simulations were used to describe structural rearrangements involved in Hsp90's conformational transitions, identifying several key interactions that may govern conformational change.[41] Lastly, structural stability analysis and protein network modeling based on atomistic simulations of Hsp90 were used to characterize the evolution of interaction networks and allosteric communication during interstate transitions, reporting a small number of conserved functional residues that may be central modulators of several functions including allosteric communication, structural stability, and cochaperone binding.[42]

It has become increasingly clear that Hsp90's highly complex regulatory mechanisms are, to a large extent, enabled by its interaction with a broad range of cochaperones that are thought to tailor the flexibility of the dimer to suite its functional needs. In this manner, cochaperones could modulate the ATPase cycle of Hsp90 by controlling the conformational transitions involved in client loading and release. Functional dynamics investigations of Hsp90's interactions with the cochaperones Aha1 and p23 demonstrated that binding of these cofactors allosterically modulate Hsp90's conformational dynamics.[43] Furthermore, analysis of the interaction networks involving Hsp90 complexes with the cofactors Cdc37, Sgt1, Rar1,[44] and p53[45] demonstrated how small-world networks involving highly connected residues at the interprotein interfaces correspond to known functional sites. Thus, far, therapeutic efforts have focused largely on targeting the nucleotide binding site. However, with the implication of cochaperone interactions

DOI: 10.1021/acs.jcim.7b00630
J. Chem. Inf. Model. 2018, 58, 383−404

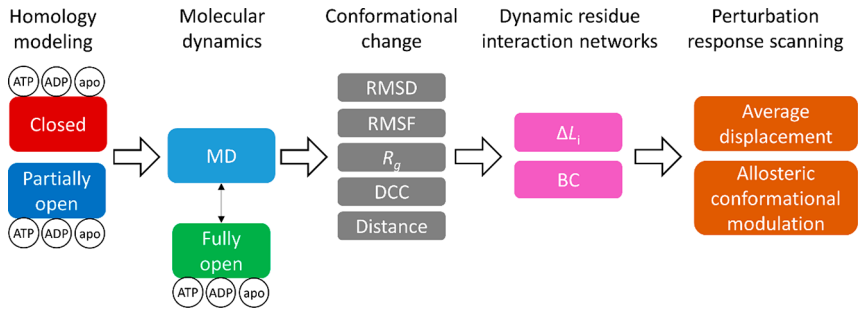

Figure 2. Schematic overview of methodology. The fully open structure was obtained from MD simulation of the partially open complex.

for client based function, drug discovery efforts are moving toward the targeting of specific cochaperone binding sites, or allosteric pockets, with the aim of disrupting Hsp90's conformational dynamics and thus its loading and release of selective clients. Interestingly, the associated allosteric regulation of Hsp90 by cochaperone interactions is believed to only occur in the cytosolic form of the protein[6,46] which would further minimize the selectivity of potential inhibitors. Progress of these therapeutic studies is limited, however, by the lack of suitable structures of human Hsp90α.

In this study, we integrated extensive all-atom MD simulations with dynamic residue network (DRN) and perturbation response scanning (PRS) analysis techniques, to probe intraprotein allostery in full length models of human Hsp90α (Figure 2). Homology modeling techniques were employed to calculate accurate 3D structural models of human cytosolic Hsp90α in conformations representative of the fully closed and partially open intermediate states. By alternating the NTD configuration of each, nucleotide bound (ATP/ADP) and apo forms of the protein were prepared as suitable starting structures for all-atom MD simulations. Analysis of the global dynamics revealed that nucleotides have a minimal effect on the conformational change in the closed complexes, but that bound ADP in the partially open (PO) structure results in significant conformational rearrangements representative of the fully open (FO) conformation and thus the opening transition. Analysis of the internal dynamics revealed that bound ATP "tenses" and structurally stabilizes the dimer regardless of its conformation, while the ADP and apo configurations "relax" the protein, imparting conformational flexibility in the protomers. DRN analysis over the MD trajectories revealed how nucleotide configuration modulates change in reachability (L_i), while betweenness centrality (BC) identified several key communication hubs that overlap with known functional sites on the protein. Comparative analysis between BC, L_i, and residue fluctuations (RMSF) revealed novel relationships between the three metrics, in which L_i and RMSF appear to behave proportionately to one another but inversely proportionate to BC. In the case of the former, the degree of correlation between L_i and RMSF may be influenced by the choice of distance cutoff used to construct the network graph, as well as the flexibility and compactness of the protein structure, as seen by the differing degrees of correlation for the closed (rigid) and FO (flexible) conformations. BC on the other hand appears less sensitive to distance cutoff, recording slightly lower correlations when compared to 1/RMSF as the distance cutoff increases, a trend that is exacerbated in the more compact CTDs. Nevertheless, the general conclusions drawn from the analyses are not sensitive to the choice of cutoff distance. In this work, results for a cutoff distance of 6.7 Å are reported unless otherwise stated. PRS analysis confirmed the functional sites identified by BC analysis, revealing several key allosteric effector residues that may be involved in modulating conformational dynamics. Included in these are residues that have been previously implicated in Aha1 binding interactions, demonstrating how the external force perturbations utilized in the PRS analysis could be used to identify naturally occurring perturbations arriving through cochaperone binding. Collectively, the data presented here provides a suitable platform for novel experimental investigations regarding human Hsp90α chaperone function and regulation.

METHODOLOGY

Homology Modeling. The 3D structure of human cytosolic Hsp90α was modeled in an open and closed conformation using the full protein sequence NP_005339.3 as the target sequence by the MODELLER[47] program. For the closed conformation, the full length cryo-EM structure of human Hsp90β in complex with ATP (PDB id 5FWK)[32] was used as a modeling template. 5FWK represents the full protein structure except for the linker between the NTD and MD (res 228−277), which due to its inherent flexibility is yet to be crystallized. For this reason, residues 230−275 were deleted from the target sequence and replaced with four glycine residues. Modeling of the open conformation required the use of a multitemplate modeling approach to ensure a "v-like" open dimer, with an extended orientation for each protomer. The canine endoplasmic reticulum paralog of Hsp90, GRP94, demonstrates a partially open "v-like" conformation with dimerization at the CTD (PDB id 2O1U)[24] and was used as the primary template. Given that 2O1U and the target sequence only share 53% sequence identity, 5FWK was used as a secondary template, providing cover for the missing region L290−R299. 2O1U lacks structural data for the ATP-lid domain (res 98−123), while 5FWK is representative of the structure with a closed ATP-lid. Thus, to ensure that the ATP-lid was modeled in its open conformation, the NTD (res 15−278) of 5FWK were excluded from the alignment file and the open ATP-lid NTD crystal structure of human Hsp90 (PDB 3T10) was used as a second template for this domain. A total of 100 models were built for each dimerized conformation (open and closed), and the respective models with the lowest normalized DOPE score (DOPE-Z score) selected for further evaluation by VERIFY3D,[48] Errat,[49] and ProSA.[50] To obtain each of these conformations in complex with ATP and ADP, the respective nucleotide's structural coordinates were extrapolated from representative crystal structures by superimposing PDBs 3T0Z[51] and 1BYQ[52] for ATP and ADP, respectively. The apo NTD was obtained by omitting nucleotide coordinate data. In this manner, a total of six human Hsp90α configurations

DOI: 10.1021/acs.jcim.7b00630
J. Chem. Inf. Model. 2018, 58, 383−404

were prepared: three in the open conformation and three in the closed conformation.

Molecular Dynamics Simulations. MD simulations were carried out on all nucleotide bound configurations of the homology models. All MD simulations were performed using GROMACS 5.1.2[53] within the CHARMM 36 force field,[54−56] using a orthorhombic periodic box with a clearance space of 1.5 nm. Water molecules were added as solvent, and modeled with the TIP3P water model. The system was neutralized using a 0.15 M NaCl concentration. Prior to production runs, all molecular systems were first energy minimized using a conjugate-gradient being energy relaxed with up to 50 000 steps of steepest-descent energy minimization and terminated when the maximum force <1000.0 kJ/(mol nm). Energy minimization was followed by equilibration, first in the *NVT* ensemble at 310 K using Berendsen temperature coupling, and then in the *NPT* ensemble at 1 atm and 310 K until the desired average pressure (1 atm) was maintained and volumetric fluctuations stabilized. All production simulations were run for a minimum of 100 ns and a maximum of 200 ns, to ensure that the backbone root-mean-square deviation (RMSD) of the protein equilibrated with a fluctuation of no more than 3 Å for at least 20 ns. Data pertaining to the protein and nucleotide were saved at 2 ps intervals for further analysis. All simulations utilized the LINCS algorithm for bond length constraints. The fast particle mesh Ewald method was used for long-range electrostatic forces, the switching function for van der Waals interactions was set to 1.0 nm, and the cutoff set to 1.2 nm. NH_3^+ and COO^- groups were used to achieve the zwitterionic form of the protein. Periodic boundary conditions were applied in all directions and the simulation time step was set to 2 fs. Duplicate simulations were carried out for all closed and FO complexes.

Dynamic Cross-Correlation. Dynamic cross-correlation (DCC) describes the correlation of motions between each C_α atom in a protein over the course of an MD trajectory. DCC is calculated based on the reduction and normalization of the $3N \times 3N$ covariance matrix (**C**). The MD-TASK[57] software suite was used to calculate DCC for each MD trajectory. **C** is constructed from the MD trajectory sampling data at 100 ps intervals, and the average deviation of each C_α atom from a mean structure representative of the trajectory length is calculated. The essential directions of correlated motions are determined by diagonalizing **C** to get the $N \times N$ correlation matrix (**Corr**):

$$\mathbf{Corr}_{ij} = \frac{\langle \Delta \boldsymbol{r}_i \cdot \Delta \boldsymbol{r}_j \rangle}{\sqrt{\langle \Delta \boldsymbol{r}_i^2 \rangle} \cdot \sqrt{\langle \Delta \boldsymbol{r}_i^2 \rangle}} \tag{1}$$

Dynamic Residue Network Analysis. To analyze inter- and intradomain communication, the protein is represented as a residue interaction network (RIN), where the C_β atoms of each residue (C_α for glycine) are treated as nodes within the network, and edges between nodes defined within a distance cut off of 6.7 Å.[58] In this manner, the RIN was constructed as a symmetric $N \times N$ matrix, where the ijth element is assigned as 1 if residue i is connected to residue j and a zero if no connection exists.

In this study, MD-TASK[57] was used to construct dynamic residue interaction networks (DRN) for each MD trajectory, in which RINs are constructed for every nth frame of the trajectory using a 200 ps time interval, to build a DRN matrix. By iterating over the DRN, each RIN is analyzed in terms of the average of shortest path length (L_{ij}) between residue i and any other residue j, and betweenness centrality (BC) of each residue. The shortest path length between two residues i and j is defined as being the number of nodes that need to be crossed to reach j from i. The average L_{ij} is then calculated as the average number of steps that the node/residue may be reached from all other residues in the RIN:

$$L_i = \frac{1}{N-1} \sum_{j=1}^{N} L_{ij} \tag{2}$$

Here, we analyze the change in reachability (ΔL_i) of each residue by monitoring how L_i shifts over the course of the MD trajectory:

$$\Delta L_i = \frac{1}{N} \sum_{m=1}^{N} (L_i^0 - L_i^n) \tag{3}$$

where L_i^0 denotes the average shortest path length for residue i at time zero and L_i^n the average shortest path length at frame n.

BC is defined as the number of shortest paths running through a node/residue for a given RIN and provides a measure of usage frequency each node during navigation of the network. Here, BC was calculated using MD-TASK based on Dijkstra's algorithm[59] and the data rescaled in the range of 0.0−1.0 to be comparable between conformers. Finally, the average BC and ΔL_i are calculated over the DRN, as this measure provides an indication of residues that experience permanent changes in ΔL_i and BC as opposed to minor fluctuations over the course of the MD trajectory.[57]

Perturbation Response Scanning. Perturbation response scanning (PRS) is a computational technique used to predict the relative response of all residues in a protein, to an external force perturbation, such as ligand binding, at a single residue. The theory of PRS has been thoroughly described in previous studies;[60−62] and the algorithm is available in the MD-TASK software suite.[57] In brief, PRS utilizes linear response theory (LRT) to approximate the shift in coordinates ($\mathbf{R}_1$) of a given protein conformation ($\mathbf{R}_0$) in response to a perturbation of the Hamiltonian.[60,63,64]

$$\Delta \mathbf{R}_1 = \langle \mathbf{R} \rangle_1 - \langle \mathbf{R} \rangle_0 \approx \frac{1}{k_B T} \langle \Delta R \Delta \mathbf{R}^T \rangle_0 \Delta \mathbf{F} = \frac{1}{k_B T} \mathbf{C} \Delta \mathbf{F} \tag{4}$$

The subscripts 0 and 1 represent the unperturbed and perturbed protein structures, respectively. The force vector **F** describes the coordinates of the inserted force perturbation on a select reside. **C** is the covariance matrix, which is constructed from a suitably equilibrated portion of the MD trajectory. Utilizing MD trajectories to construct **C** is advantageous in that the movement of all atoms of the protein are taken into consideration; however, previous studies have shown that to accurately construct the Hessian from MD data, short enough coordinate trajectories (20−40 ns) must be used to ensure that data is sampled from a single potential well.[65,66] Furthermore, it is imperative that the trajectory segment used is at equilibrium or quasi-equilibrium. Here, 20 ns trajectory segments with a backbone RMSD fluctuation of no more than 2.5 Å were used to construct **C**. The deviation of each atom from a mean structure over the 20 ns was calculated as $\Delta \mathbf{R}_j(t) = \mathbf{R}_j(t) - \mathbf{R}_j(t)$ and stored in a matrix $\Delta \mathbf{R}$, and the covariance matrix **C**, is calculated from $\Delta \mathbf{R} \Delta \mathbf{R}^T$. For each PRS experiment, the initial and final structures (states 0 and 1) were defined as follows:

DOI: 10.1021/acs.jcim.7b00630
J. Chem. Inf. Model. 2018, 58, 383−404

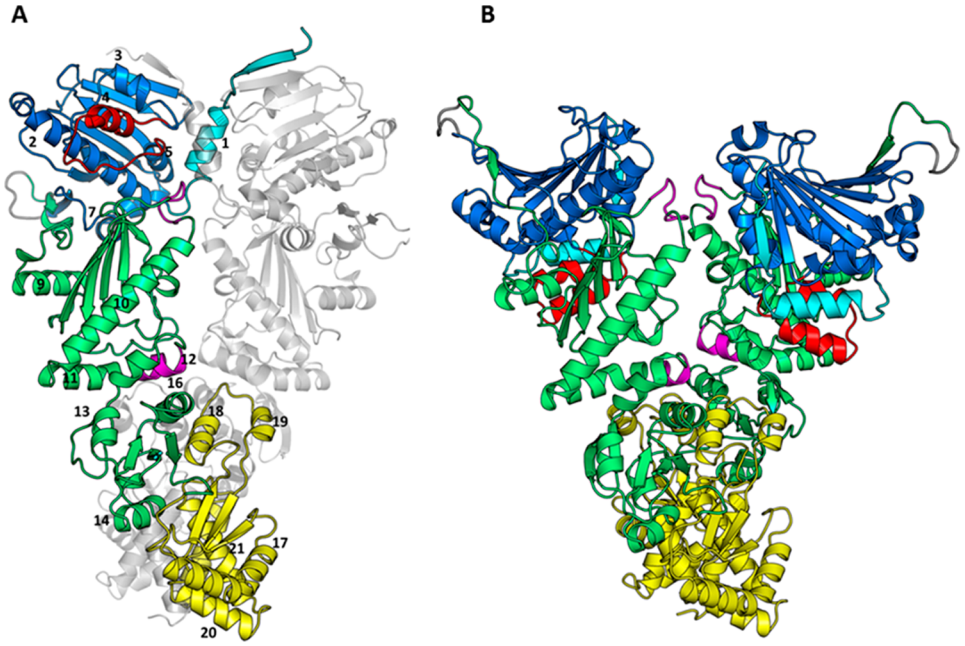

Figure 3. 3D Illustration of human Hsp90α homology models: (A) fully closed conformation, (B) partially open conformation. Indicated are the locations for the NTD (blue); charged linker (gray); M-domain (green); CTD (yellow); ß-strand$_1$–helix$_1$ interface (cyan); ATP-lid (red); and M-domain/CTD hinge (magenta). Helices are labeled according to the numbering convention used throughout the text.

The first frame of the equilibrated MD trajectory segment was set as state 0. For the open to closed transitions, the final structure (state 1) was set to the equilibrated structure of the ATP bound closed configuration. Conversely, for the closed to open transitions, the final structure was set to the equilibrated ADP bound open conformation after 200 ns. The coordinates of state 1 were superimposed on state 0 using a whole protein approach with the Kabsch algorithm[67] and the experimental difference vector calculated (ΔS). Each residue in the initial state was sequentially perturbed with 250 fictitious forces of random direction. For each residue i, MD-TASK assesses the quality of the response vector (ΔR_k) using the Pearson's correlation coefficient by correlating ΔR_k with the experimental displacements averaged over all affected residues k:

$$C_i = \frac{\sum_{k=1}^{N} [(\Delta R_k)^i - (\overline{\Delta R})^i](\Delta S_k - \overline{\Delta S})}{(N-1)\sigma_R \sigma_S} \quad (5)$$

The overbar denotes the average, and ΔS_k, the experimental displacements, and σ_S and σ_R are the respective root-mean-square values. Thus, for each residue i, ΔR_k is compared to ΔS_k 250 times under a unique force each time, and the goodness of fit quantified with the Pearson's correlation coefficient (C_i). A C_i value close to 1 implies a good agreement with the experimental change and a C_i value close to 0 indicates little or no agreement. In each case only the maximum C_i is recorded for each residue. We have previously discussed and shown the reproducibility of this approach with large multidomain proteins with complex rotational and translational conformational restructuring.[62]

RESULTS AND DISCUSSION

Homology Modeling. Structures of human Hsp90α in closed and partially open v-like conformations were obtained by homology modeling (Figure 3). In each case 100 unique homology models were calculated and ranked by normalized DOPE-Z score. The normalized DOPE-Z score is an atomic distance-displacement statistical potential used to evaluate the fold of a model and is dependent on a sample structure of a native protein.[68,69] A value less than −0.5 is deemed an accurate representation of the native structure, and the lowest scoring models were selected for further model evaluation and verification. Table S1 summarizes the results of the best scoring models after separate model evaluation with Verify3D, Errat, and ProSA techniques. Verify3D is an online Web server that determines the relative compatibility of an atomic coordinate structure (3D) with its own amino acid sequence (1D), assigning structural classes based on secondary structure, location, and local environment, comparing the results with known good structures.[70,71] The percentage of residues within the protein that score more than 0.2 is reported, and a minimum of 80% is required to pass model evaluation. Errat is a program that analyzes the statistics of all nonbonded interactions between carbon, nitrogen, and oxygen atoms reporting the percentage of residues that fall below a rejection confidence level of 95%.[49] The ProSA Web server calculates the overall quality of a protein structure based on a Z-score which indicates the goodness of fit between the modeled structure and native structures of a similar size.[50] Both the selected open and closed homology models pass each of these evaluation tests, recording scores in the good to very good range (Table S1). Model evaluation was carried out before and after energy minimization, to assess the impact of possible bad contacts within the structure. Erroneous regions highlighted in the preminimized structures are mostly confined to loop regions, particularly the missing linker region between the NTD and the M-domain, and all improve post energy minimization (Table S1). The final models selected proving suitable starting structures for long-range MD simulations.

Effect of Nucleotide Binding on Conformational Change. The NTD nucleotide bound configuration (ATP/ADP/apo) has been intricately coupled with the modulation of conformational dynamics in Hsp90's chaperone cycle (Figure

DOI: 10.1021/acs.jcim.7b00630
J. Chem. Inf. Model. 2018, 58, 383−404

Table 1. Summary of MD Simulations for the Closed, Partially Open, and Fully Open Complexes[a]

complex	initial structure	length	label	box dimensions (nm^3)	total atoms
closed-ATP*	closed HM	100 ns	Closed-ATP		
closed-ADP*			Closed-ADP	7.89 × 10.49 × 12.69	174159
closed-apo*			Closed-apo		
partially open-ATP			PO-ATP		
partially open-ADP	PO HM	200 ns	PO-ADP	9.43 × 8.86 × 12.40	177893
partially open-apo			PO-apo		
fully open-ATP*	PO-ADP		FO-ATP		
fully open-ADP*	(200 ns)	200 ns	FO-ADP	10.37 × 12.68 × 12.49	259331
fully open-apo*			FO-apo		

[a]HM homology model; PO partially open; FO fully open; * duplicated trajectories..

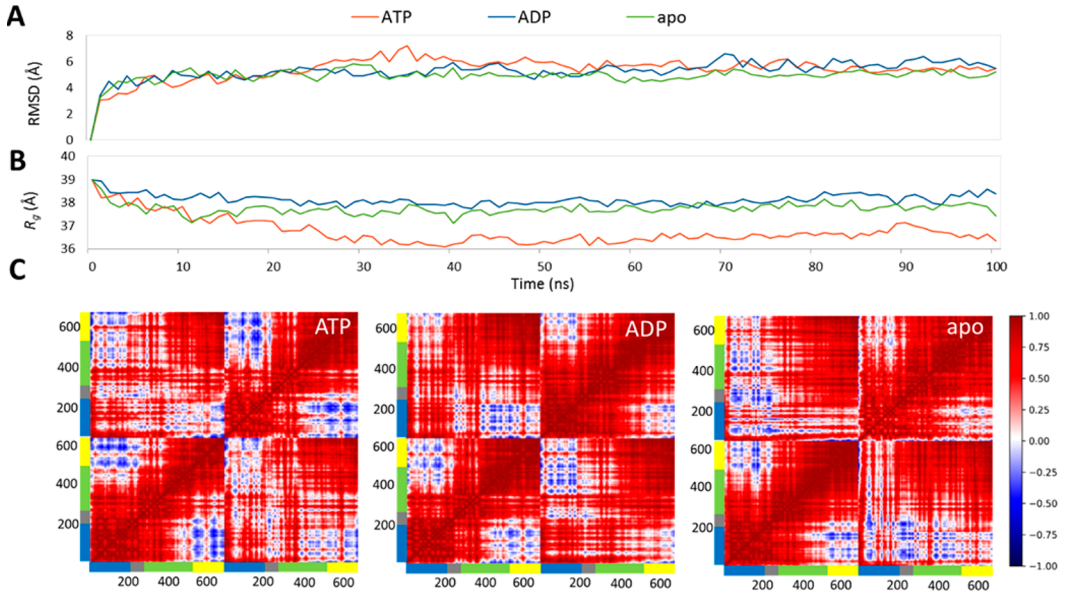

Figure 4. Global conformational dynamics metrics for the closed conformation complexes: (A) backbone RMSD; (B) radius of gyration; (C) DCC heat maps showing correlated motions (positive) in red and anticorrelated motions (negative) in blue. The color bar accompanying each heat map represents each functional domain: NTD (blue), linker (gray), M-domain (green), and CTD (yellow).

1). To determine the relative effect of bound nucleotide on the conformational dynamics (opening and closing transitions) of human Hsp90, all-atom MD simulations in explicit water were carried out on nucleotide bound (ATP/ADP) and apo closed, PO, and FO complexes, in a total of nine unique simulation runs (Table 1). Duplicate MD simulations were carried out for the closed and FO complexes to confirm MD convergence, with a total simulation time of 1.8 μs for 12 separate MD runs (Table 1 (starred complexes), Figure S2). The closed and PO simulations were initiated based on the homology models, while the FO simulations were based on a structure extracted from the PO-ADP MD trajectory. The resultant trajectories were analyzed in terms of their backbone RMSD, residue root-mean-square-fluctuations (RMSF), radius of gyration (R_g), interprotomer distance, dynamic cross-correlation (DCC) of atomic motions, and observed conformational changes.

Closed Complexes. Backbone RMSD analysis indicates fairly stable structures over 100 ns for all three closed conformation complexes, with RMSD values converging around 5−6 Å (Figure 4A). RMSF analysis for these trajectories (Figure S3) reveals prominent NTD fluctuations surrounding residues belonging to the loop R60-E75, the ATP-lid (res 112−136), and the charged linker (res 220−282), with subtle differences between the two protomers. The only notable difference between the nucleotide configurations are slightly larger values for the ATP complex, an observation that is in agreement with a previous MD study on yeast Hsp90.[34] Despite RMSD convergence and similar RMSF values between the three configurations, visual inspection of the final structures (100 ns) reveals subtle differences in the NTDs of each complex when compared to their initial structures (0 ns), in which the NTD of the ATP complex become more compact compared to the NTDs of ADP and apo complexes (Figure S4). The R_g over the MD trajectory provides a metric for evaluating the degree of compactness of a protein of interest.[72] R_g analysis for the closed complexes shows an initial decrease for the ATP complex which eventually stabilizes around 36.5 Å (Figure 4B), suggesting a tightening of the dimers around the central axis. The ADP and apo complexes show a smaller initial decrease compared to the ATP complex, both stabilizing around 38.5 Å, suggesting these complexes to be more "relaxed" around the central axis. The apparent compactness of the ATP complex is also confirmed when analyzing the MD trajectories in terms of correlated C_β atom motions (eq 1). In this analysis, each correlation matrix (Figure 4C) represents the correlation between any two C_β atoms over the course of an MD trajectory. Positive values approaching 1 describe correlated motions (in the same direction), and negative values close to −1 describe

DOI: 10.1021/acs.jcim.7b00630
J. Chem. Inf. Model. 2018, 58, 383−404

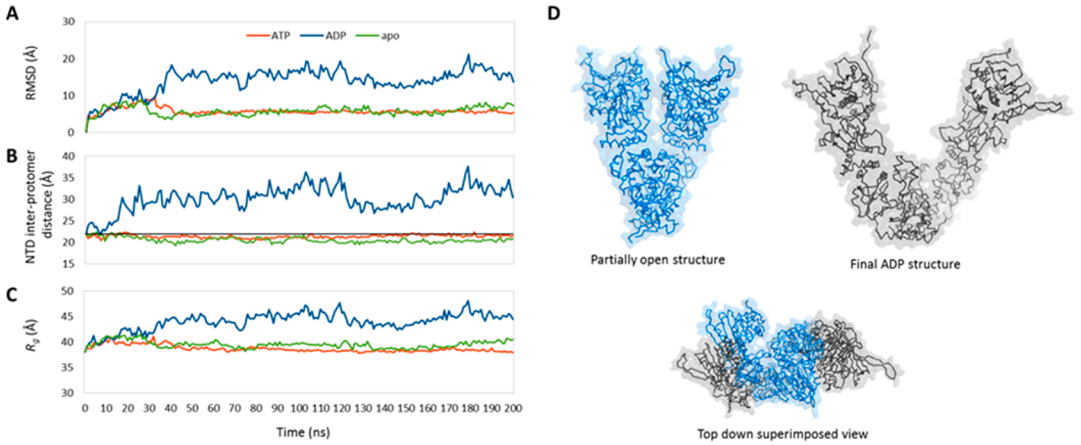

Figure 5. Global conformational dynamics metrics for the partially open conformation complexes: (A) backbone RMSD, (B) NTD interprotomer distance (black line represents the distance at 0 ns), (C) R_g plots, (D) 3D illustration of dimer opening in the PO-ADP complex, showing the initial partially open structure (blue) and the final structure after MD simulation (gray).

anticorrelated motions (in opposite directions). In the ATP complex, strong anticorrelation is observed between the NTD and CTD within and between individual protomers, suggesting these domains to have anticorrelated motions either toward or away from each other in the presence of ATP. The degree of anticorrelation between these domains is reduced in the ADP and apo complexes, especially in protomer 2, supporting the hypothesis that these complexes resemble more relaxed structures. Protomer uncoupling at the NTD precedes transition toward the open state. Looking at the motions between the NTDs of each protomer, positive correlated motions are observed between the NTDs of the nucleotide bound complexes, suggesting that the NTDs move in a concerted fashion relative to one another. Strikingly, the converse is observed for the apo structure, in which the NTDs show anticorrelated motions relative to one another suggesting movement in opposite directions, and possibly indicative of protomer uncoupling. We note that these observations are unlikely to be attributed to a lack of MD convergence, as replicate DCC heat maps computed for separate trajectories demonstrate highly reproducible results (Figure S5). Furthermore, we suggest that the differential behavior observed for the two protomers may be evidence of previously reported asymmetric conformational dynamics of Hsp90,[14,73] a characteristic that is also observed in the DRN and PRS analyses presented and discussed in more detail later.

Previous experimental studies have shown evidence that Hsp90's conformational transition from the closed ATP bound "tense" state to the open "relaxed" state can only be achieved after ATP hydrolysis and the subsequent release of ADP from the NTD.[6] The MD data presented here suggests that 100 ns runs are insufficient to observe the expected global restructuring required for the opening transition with similar final structures observed for all three complexes (Figure S4). Nevertheless, the data presented do demonstrate that the complex is amenable to subtle structural changes and deviation from the initial structure under the different NTD configurations. Bound ATP appears to enhance the NTD-CTD "compactness" of the complex, providing evidence in agreement that this complex favors the closed "tense" state,[6,17,73,74] while the ADP and apo complexes appear to relax the NTD and CTD relative to one another, possibly in preparation for the opening transition.

Partially Open Complexes. The PO complexes of human Hsp90α were calculated based primarily on the canine Grp94 template (PDB id 2O1U), which is representative of a partially open structure that may represent the native conformation of the protein in the absence of bound client proteins or cofactors.[24] The atomic coordinates for the ATP-lid are missing from 2O1U, and as such, these complexes were modeled with the ATP-lid in the open configuration, providing a putative intermediate structure between the closed catalytically active state and the native inactive fully open state.

The backbone RMSD plots of the PO complexes (Figure 5A) indicate minor conformational restructuring within the first 35 ns, after which the ATP and apo complexes stabilize, converging to a value around 5 Å, while the ADP complex undergoes extensive conformational fluctuations, without equilibrating over the 200 ns simulation. Superimposing the CTDs of the final structures with the initial PO structure shows that each complex configuration yields a unique final structure after the 200 ns MD simulation (Figure S6). As expected, the ATP complex undergoes minor conformational change in which the NTDs are reoriented toward the M-domain of the opposite protomer (Figure S6 red). This reorientation appears to tighten the two protomers, in line with conformational rearrangements thought to be necessary for catalytic activation.[16,26] The ADP complex appears to undergo extensive conformational restructuring, whereby the protomers disengage from one another in a distinct opening of the molecular clamp. Indeed, the final PO-ADP structure closely resembles an open v-like (Figure 5D), the backbone RMSD deviating only 8.23 Å from the similarly structured bacterial Hsp90 HtpG (PDB id 2IOQ)[23] after 3D superimposition (Figure S6B). Like the PO-ATP complex, the PO-apo complex also shows minor deviation from the initial structure, the only notable conformational change being the NTD of the second protomer, which appears to relax and extend in an upward flexing motion away from the M-domain of the opposite protomer (Figure S6 green). Measuring the time evolution of NTD interprotomer distance, defined by the distance between the center of mass of each the NTDs, over the course of each MD simulation (Figure 5B) reveals that the protomers of the PO-ADP complex fully uncouple after ~20 ns, the interprotomer distance increasing by ~10 Å, to fluctuate around 30 Å. In contrast, both the ATP and

DOI: 10.1021/acs.jcim.7b00630
J. Chem. Inf. Model. 2018, 58, 383−404

apo complexes maintain their NTD interprotomer distance, fluctuating around 21 Å.

RMSF analysis of the PO complexes (Figure S7) shows an elevated degree of residue fluctuation in the NTDs of all three complexes, with slightly higher fluctuations observed for the ADP complex. Notable NTD fluctuations include the N-terminal β-strand$_1$ (res 15−26), β-sheets 3−5 (res 65−75, 160−80), the ATP-lid (res 112−136), and the charged linker (res 210−290). A notable difference between the different PO configurations is observed in the M-domain (res 288−549), where fluctuations are increased for the ADP complex, particularly the catalytic loop region (res 391−406). All three complexes show similar residue fluctuations at the CTD; however, the ADP complex once again experiences higher fluctuations, this time at helix$_{18}$ and helix$_{19}$ (res 601−632). Collectively this data suggests that the ADP complex is more flexible than the ATP and apo complexes, experiencing fluctuations in all three subdomains which may be evidence of a relaxed ADP state. This apparent increase in flexibility for the ADP complex may be an important structural characteristic for the destabilization of anchoring interprotomer interactions in the M and CTDs, allowing the protomers to easily disengage as seen in the final structure of the ADP bound complex (Figure 5D).The converse may be true for the PO-ATP and PO-apo complexes, in which protomer rigidity may help maintain interprotomer interactions, thus stabilizing and favoring the closed state. R_g analysis for these complexes supports this observation (Figure 5C), in which the PO-ADP complex becomes considerably less compact over time, increasing in value to fluctuate around 45.0 Å at approximately the same time point that the protomers first disengage (Figure 5B). In contrast, the PO-ATP and PO-apo complexes maintain their original structures, fluctuating around 38.0 Å, the former becoming slightly more compact than the latter. Looking at the interprotomer interactions present in the final MD simulation structures, the only interactions conserved in all three complexes are those involved in CTD dimerization, the notable difference being helix$_{18}$ (res 601−632). In the initial closed and PO structures, helix$_{18}$ is seen to form intimate interactions with the identical residues in the opposite protomer, forming an important interface between the protomers. Despite minor fluctuations of these residues over the course of the MD simulations (Figure S7), both the apo and ATP complexes appear to retain this interprotomer interaction, while in the ADP complex they are completely abolished, allowing helix$_{18}$ and helix$_{19}$ to fold back toward their respective protomers. The CTD has been previously implicated in the allosteric modulation of dimerization in yeast Hsp90.[34,36,75,76] This data could describe how ADP may allosterically modulate conformational dynamics, in which it increases protomer flexibility, allowing the NTDs to become extended triggering disengagement of helix$_{18-19}$ interface, which in turn causes further destabilization of other interprotomer interactions in the M-domains, resulting in a transition to the open state.

Fully Open v-like Complexes. All-atom MD simulations of the PO complexes revealed drastic conformational changes in the ADP configuration that closely resembled the FO v-like conformation (Figure S6B). This structure provided a suitable starting point for further MD investigations regarding the effect of bound nucleotide on the conformational dynamics of the FO conformation. As such, the final structure of the PO-ADP complex was selected from the 200 ns trajectory, and FO-ATP, FO-ADP, and FO-apo complexes prepared in the same manner as the previous two conformations, and each complex submitted to 200 ns MD simulations.

The RMSD plots of the fully open complexes (Figure S8A) indicate minor backbone fluctuations for the ATP and apo complexes, the RMSD values converging around 6 Å. However, the FO-ADP complex appears to undergo large conformational changes at the 100 ns time point, which correspond to a slight increase in NTD interprotomer distance (~2 Å) (Figure S8B). RMSF analysis of all three complexes (Figure S9) reveals very similar residue fluctuation profiles to the PO complexes (Figure S7), where the NTD and M-domains experience higher fluctuations compared to the CTD. Comparing the final structures of each complex, the only noticeable difference is observed for the ATP complex in which the NTDs appear to reorient inward, toward their respective M-domains, a movement that may be indicative of an early closing motion.

Overall, the data presented here demonstrate that major conformational dynamics are experienced for the PO complexes in response to the ligand bound state of the NTD, while more subtle structural rearrangements are experienced by the closed and FO complexes. In each case, ATP appears to confer structural rigidity and tensing of the dimer, while ADP enables a more relaxed flexible complex. The apo complex engenders opposing correlated motions in the closed complexes, while it has little or no effect on the PO and FO complexes which appear largely stable. This contrasting behavior may be in agreement with reports of stochastic dynamics observed for the apo protein.[74,77,78] While these findings are in agreement with several previous studies,[6,73,74] the only conformational transition observed within the MD simulation time scales used in this study was the opening transition of the PO-ADP bound complex. To probe our data for further insights regarding nucleotide modulation of interstate transition, the MD trajectories of the closed and FO complexes were subjected to DRN analysis to investigate the effect of bound nucleotide on intraprotein communication, as well as PRS analysis to identify single residues involved in modulating interstate conversion.

Dynamic Residue Network Analysis. In this analysis, each Hsp90 complex is treated as a network of residues, where the C_β (C_α for glycine residues) atoms for each residue are considered to be nodes in the network, and the edges between nodes established based on a separation cutoff distance of 6.7 Å.[58] In this manner, DRNs are calculated for each trajectory, and the resultant matrices analyzed in terms of the shortest path (L) and betweenness centrality (BC). Briefly L_{ij} is the number of connections (edges) utilized to reach node/residue i from j, using the shortest possible path. L_i is thus the average path length for node i and is calculated as the average number of steps that the node may be reached from all other nodes in the network. Here, we monitor the change in L_i (ΔL_i) in response to the ligand bound configuration of the NTD and interpret large ΔL_i as sites on the protein that may be important for inducing intraprotein communication.[79] BC is associated with L in that it is measure of the number of shortest paths passing through a given residue, and thus the usage frequency of a residue in cross network communication, where high usage residues are considered to potentially play a role in controlling intraprotein communication.[79] The efficiency of this method for the calculation and analysis of BC and ΔL_i along the MD simulation has previously been shown in a recent study on single nucleotide variants in the renin−angiotensinogen

DOI: 10.1021/acs.jcim.7b00630
J. Chem. Inf. Model. 2018, 58, 383−404

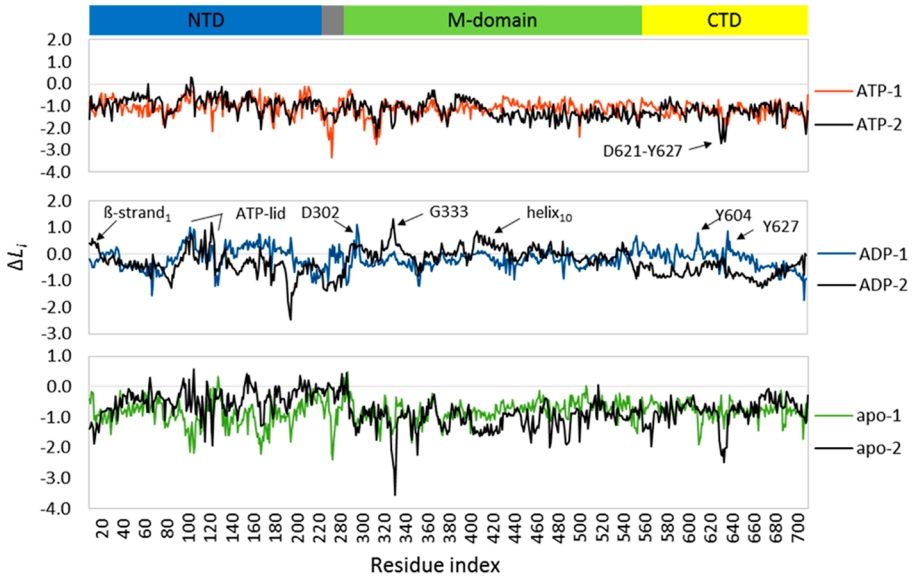

Figure 6. Change in reachability (ΔL_i) plots for the closed conformation complexes. Protomer 1 is colored by NTD configuration (ATP red, ADP blue, apo green), and protomer 2 is in black.

complex.[80] Here, we apply this analysis technique to each of the closed and FO complex configurations.

Nucleotides Modulate Long-Range Residue Reachability. The ΔL_i profiles for the closed complexes (Figure 6) show that the ATP and apo complexes experience mostly negative ΔL_i values over the length of the protein, while the ADP complex experiences both positive and negative change. Negative ΔL_i can be described as a shortening of the average path length between all residues and residue *i*, while positive ΔL_i values indicate increased path lengths. Thus, the negative ΔL_i observed in the ATP and apo complexes may suggest these conditions favor more compact structures, resulting in decreased path lengths. Conversely, the increased path lengths observed for the ADP complex may suggest a more relaxed elongated structure. Indeed, this explanation of the findings is in agreement with our conformational dynamics results, confirming structural tensing and relaxing under ATP and ADP conditions, respectively.

Regions of the protein that display elevated ΔL_i point to structural elements that are important for inducing intraprotein communication. Looking at the respective ΔL_i profiles in more detail, it is interesting to note a differential degree of change in some regions depending on the ligand bound configuration of the NTD. Residues residing in ß-strand$_1$ (res 15−26) and the ATP-lid (res 112−136), residues D302, S330-L335, helix$_{10}$ (res 407−427), and residues neighboring Y604 and Y627 all record sharp positive ΔL_i in the presence of ADP, and negative changes for ATP. ß-strand$_1$ swapping between protomers contributes to the stabilization of NTD dimerization,[5,17,81] and its deletion has been shown to affect ATPase activity in mitochondrial and yeast Hsp90 homologues.[82,83] The ATP-lid is intricately implicated in the progression of conformational change, acting as a trigger for NTD dimerization in response to bound ATP.[5,17,30,84] Helix$_{10}$ has been previously implicated in nucleotide driven allosteric signal propagation between the NTD and M-domain in *E. coli* HtpG.[40] Residues Y604 and D621-Y627 reside in helix$_{18}$ and helix$_{19}$ respectively, and undergo large negative ΔL_i in the ATP and apo complexes, but display positive ΔL_i in the ADP complex, suggesting a tighter binding of these interface elements in the ATP and apo complexes. This observation is in agreement with the conformational dynamics analysis of the PO structures in which interactions between these residues from either protomer are lost in the presence of ADP, but are retained in the ATP and apo complexes.

Studying the respective ΔL_i profiles for the FO complexes (Figure 7) reveals largely negative ΔL_i for FO-ATP, while ΔL_i for FO-ADP and FO-apo fluctuate. As seen in the closed complexes, certain regions of the protein respond differentially in response to the bound configuration of the NTD. Here, residues E200−K224, forming ß-strand$_8$ located at the interface between the NTD and the charged linker, experience negative ΔL_i in the ATP complex, and positive ΔL_i for the ADP and apo configurations, demonstrating a reduced flexibility in this region when ATP is present. In fact, these residues have been directly implicated in the regulation of the human Hsp90α ATPase cycle, whereby mutations to select residues in this region lead to increased NTD flexibility, resulting in severely altered chaperone activity and a shift in the conformational equilibrium in favor of the open state.[20] In the M-domain, residues R367−E380 and L396−Q404 are in close spatial proximity to one another, and all experience sharp positive ΔL_i in the presence of ADP compared to ATP. Positioned at the NTD/M-domain interface, they have also been reported to form a nucleotide sensitive hinge, implicated in allosteric signal propagation from the NTD to the M-domain.[39,42] In the CTD, both helix$_{18}$ and helix$_{19}$ experience positive ΔL_i in all three complexes; however, FO-ADP experiences greater change, once again suggesting looser interactions under these conditions.

We note that ΔL_i differences between protomers is observed in both the closed and FO complexes, an observation that suggests the possibility for asymmetrical modulation of protein dynamics. In the closed complexes, notable differences in ΔL_i values between protomers are observed for the ADP and apo complexes, while large contrasting ΔL_i values are recorded in the ß-stand$_1$, helix$_1$, and the ATP-lid regions of all three open complexes. This differential modulation is unlikely to arise due to asymmetry in the starting structures, with backbone superimposition of the protomers yielding RMSD values of 0.8 and 3.1 Å for the closed and FO conformations respectively,

DOI: 10.1021/acs.jcim.7b00630
J. Chem. Inf. Model. 2018, 58, 383−404

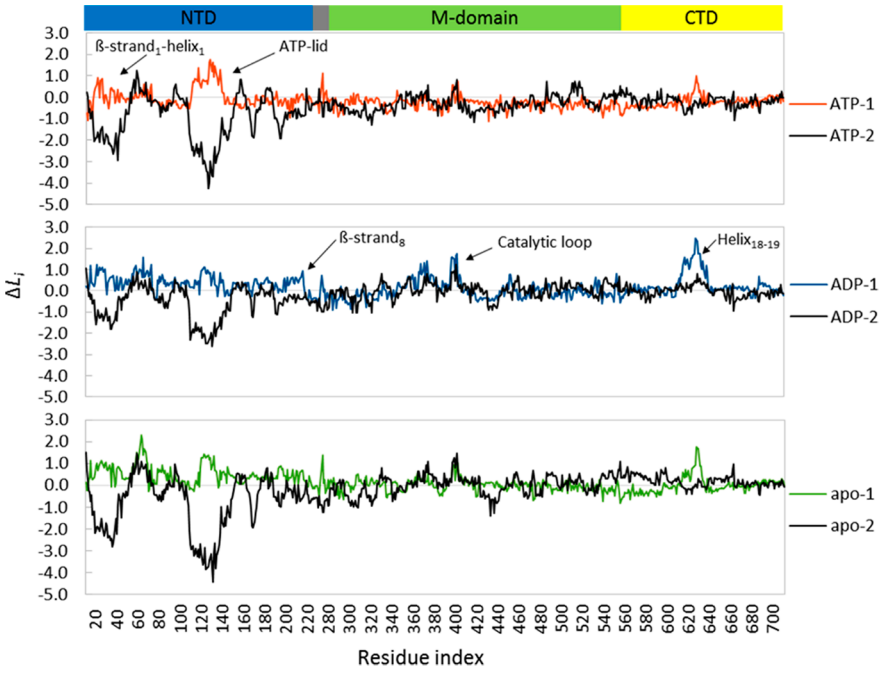

Figure 7. Change in reachability (ΔL_i) of each residue for the fully open complexes. Protomer 1 is colored by NTD configuration (ATP red, ADP blue, apo green), and protomer 2 is in black.

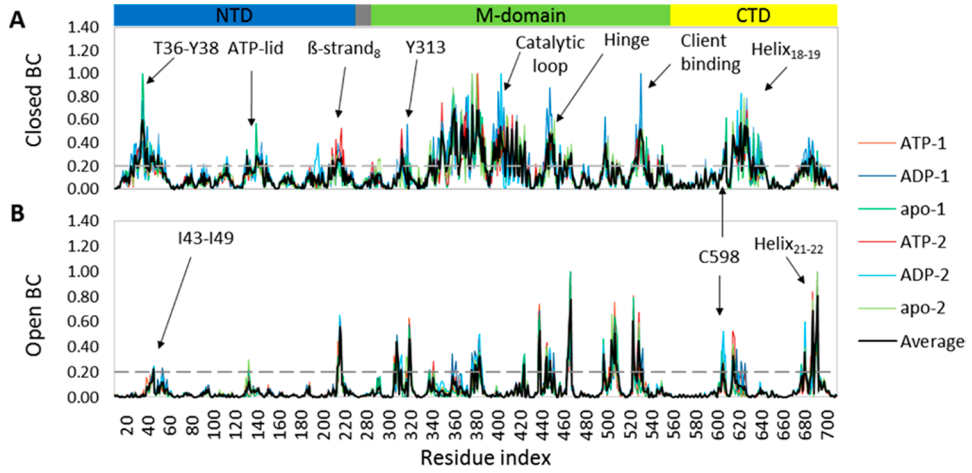

Figure 8. Betweenness centrality (BC) profiles: showing regions in the (A) closed and (B) open complexes that may constitute putative communication hubs. Dashed gray lines indicates the peak residue threshold.

while the NTDs of the FO conformation superimpose with an RMSD value of 1.2 Å, indicating a high degree of symmetry between protomers 1 and 2 for both conformations. Furthermore, ΔL_i analysis on replicate trajectories demonstrated highly reproducible results (Figure S10), eliminating MD convergence as a possible cause of asymmetry. As such, we suggest that this differential behavior may be further evidence of previously reported asymmetrical protomer dynamics of the protein in response to the nucleotide bound configuration.[14,73,83]

Overall, ΔL_i provides a unique metric for monitoring the effect of nucleotide modulation on local and global restructuring and its implication on long-range communication in Hsp90, highlighting several regions of the protein that may be involved in steering conformational change. Here, the analysis confirms the tensing effect of ATP, with the protomers of both conformations experiencing negative ΔL_i values. Conversely, protomer relaxation afforded by ADP binding is also confirmed, with the average path length increasing in both ADP bound conformations. Regions that experience large ΔL_i are most notable in the open complexes, and include residues belonging to the functionally important ß-strand$_1$, helix$_1$, ATP-lid, and catalytic loop,[5,17,84] as well as the helix$_{18}$/helix$_{19}$ CTD interface.

Betweenness Centrality Points to Putative Communication Hubs. BC has been shown to be an effective measure for identifying functional residues implicated in the control of intraprotein communication,[79,80] as well as protein−ligand[85] and protein−protein binding sites[86,87] (see review 88 for other examples). Here, BC is calculated for the closed and FO complexes to identify individual/groups of residues important for intra- and interprotomer communication.

The respective BC profiles of both conformations (Figure 8) reveal that bound nucleotide has little impact on modulating

DOI: 10.1021/acs.jcim.7b00630
J. Chem. Inf. Model. 2018, 58, 383−404

Table 2. Summary of Residues with High BC for the Closed and Open States

state	NTD	M-domain	CTD
closed	I34−D54; M130−A145; I206−L220	F312−N318; L351−V388; L396−F428; F441−E451; Y493−E497; Y520−V530; L541−K546	C598−T601; W606−K632; L666−N686
open	I43−I49; M130−F134; S211−I214	F312−Y313; H323−L324; L340−L341; P344−R345; I361−Y364; R367−F369; I378−G387; L423−F424; F437−Y438; F441−E451; L462−Y465; I494; Q501−F507; Y520−Y528	C598−T601; T607−L619; L671; L678; D680−Q682

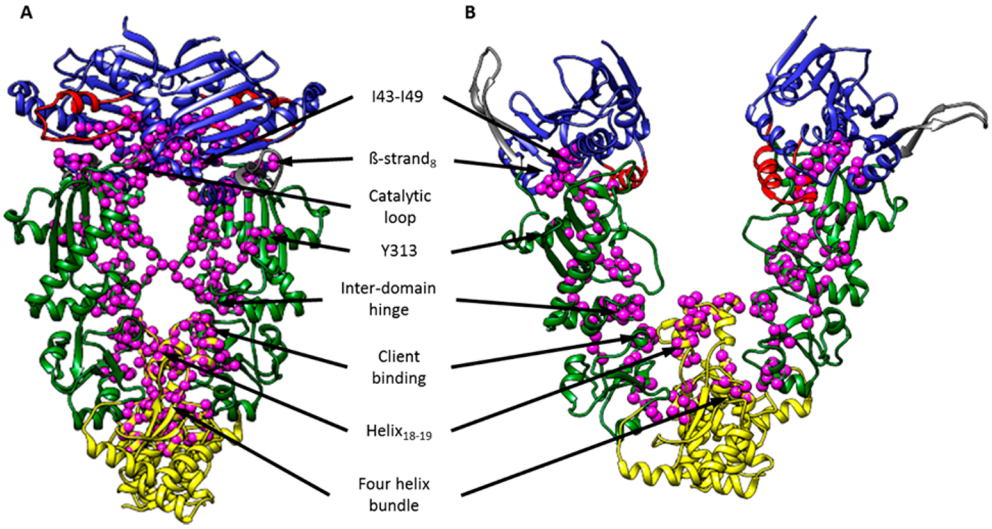

Figure 9. Structural mapping of high BC residues: (A) closed complex and (B) fully open complex. Showing peak residues as magenta spheres.

communication hubs in either conformation, with similar trends observed for all three configurations. Thus, to simplify data presentation, the average BC over all three configurations for each conformation is shown (Figure 8 black curves). Peak locations in each conformation describe residues with high BC and thus high frequencies of usage in intraprotein communication. As previously mentioned, BC for a given residue *i* is a measure of the number of shortest paths that visit *i*, and points to locations on the protein that may be important communication hubs given their high frequency of usage. For the closed conformation complexes, the inherent compactness and rigidity of the structure, coupled with an increased number of intra- and interprotomer contacts, is expected to influence BC by increasing the number of possible shortest paths in the network. This is a scenario that will likely lead to an increase in the number of possible communication hubs when compared to the FO complexes, where the protomers are more dynamic and only interact at the CTD. Our results are in agreement with this expectation, with peak residues for the closed complexes being tightly grouped, listing residue regions rather than select residues as seen in the FO complexes (Figure 8A and B). Nevertheless, both conformations share several overlapping peak residues that correlate well with known functional residues, particularly those involved in regulating ATPase activity and conformational dynamics. Peak residues listed by BC are summarized in Table 2 and are mapped to their respective 3D structures in Figure 9, and their respective functional importance is discussed below.

Starting with the NTD, phosphorylation and mutation studies have linked T36 and Y38 to ATPase regulation and altered binding of cochaperones Aha1 and Cdc37,[84,89,90] while computational studies have implicated both residues in interdomain signal propagation.[34,75,91] These residues are only selected in the closed complexes where they help stabilize NTD dimerization by contributing to crucial interactions with the catalytic loop (S391−S406) and residues R46−I49.[16,17] Residues I43−I49 are listed in both conformations, and mutation studies have shown that E47A abolishes ATP hydrolysis suggesting a catalytic function *in vivo*.[52] In the closed conformation, E47A would have a negative impact on catalytic loop interactions and thus decrease ATPase activity. In the open state, I43−I49 are positioned in closed proximity to the open ATP-lid, presumably helping to stabilize it in the configuration. Furthermore, BC also lists lid residues M130−F134 in both conformations. In the open complex, these residues are uniquely positioned over I43−I49, while in the closed complex, they are positioned over residues S53 and D54, which together form a hydrophobic patch known to be involved in ATP-lid stabilization.[84] In sum, these findings point to I43−I49 and M130−F134 as crucial communication hubs in both conformational states.

Next, residues I206−L220 of ß-strand$_8$ and helix$_7$ are located at the interface between the NTD and charged linker and have been implicated in chaperone secretion and modulation of the ATPase where I218A and L220A mutations are thought to alter the charged linker's topology, causing reductions in cochaperone association and *in vivo* cell death.[20] Of these residues, only S211−I214 are listed in both conformations, and we note that, in the closed complexes, ATP records higher BC values for these residues than the ADP and apo configurations. The apparent loss of BC in the ADP and apo complexes is significant in that the mutation I218A has also been shown to impact conformational dynamics, shifting the conformational equilibrium in favor of the open state.[92] It is possible that I206−L220 may act as a crucial communication hub capable of sensing bound nucleotide at the NTD. Under rigid ATP conditions I206−I220 may help stabilize the complex in a closed conformation. Eventual ATP-hydrolysis and subsequent protomer relaxation in response to ADP binding may

DOI: 10.1021/acs.jcim.7b00630
J. Chem. Inf. Model. 2018, 58, 383−404

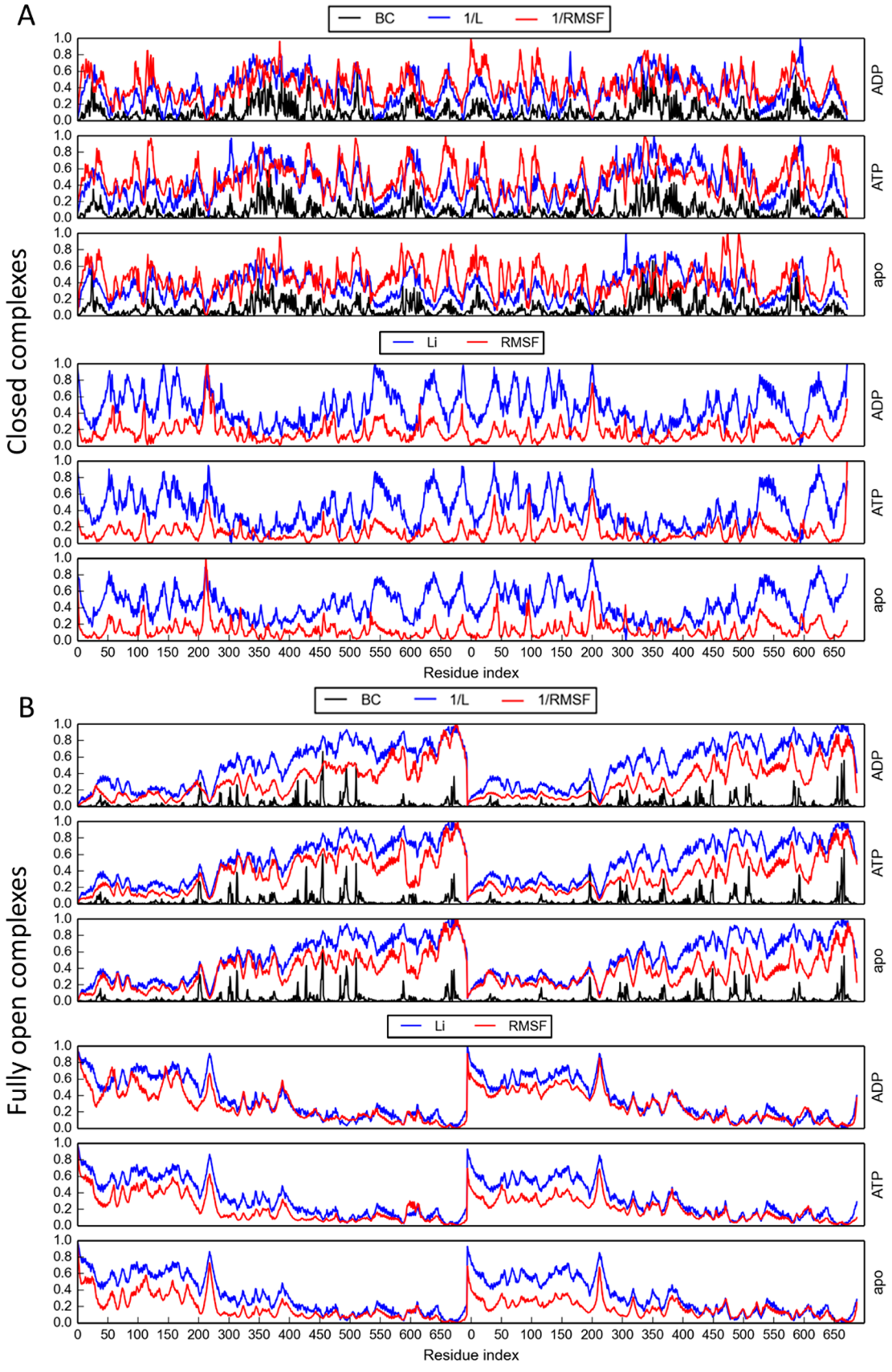

Figure 10. Graphical comparison of BC, L_i, and RMSF for (A) the closed and (B) fully open conformation complexes, showing the inverse relationship between BC-L_i^{-1} and BC-RMSF^{-1} (upper panel) and the proportional relationship between L_i and RMSF (lower panel).

DOI: 10.1021/acs.jcim.7b00630
J. Chem. Inf. Model. 2018, 58, 383−404

Table 3. Comparison of BC, ΔL_i^{-1}, and $RMSF^{-1}$ by Pearson's Correlation Coefficient, for Each Separate Protomer[a]

			Protomer 1				Protomer 2			
			NTD	MD	CTD	whole	NTD	MD	CTD	whole
closed	BC vs L^{-1}	ADP	0.80	0.70	0.83	0.74	0.76	0.74	0.73	0.73
		ATP	0.79	0.66	0.81	0.70	0.71	0.64	0.75	0.66
		apo	0.74	0.69	0.70	0.70	0.76	0.61	0.66	0.64
	BC vs $RMSF^{-1}$	ADP	0.53	0.55	0.66	0.57	0.6	0.51	0.65	0.51
		ATP	0.57	0.55	0.57	0.55	0.55	0.44	0.53	0.48
		apo	0.60	0.37	0.53	0.47	0.58	0.41	0.55	0.45
	RMSF vs L	ADP	0.53	0.71	0.69	0.62	0.63	0.70	0.74	0.62
		ATP	0.63	0.75	0.73	0.66	0.69	0.70	0.36	0.57
		apo	0.80	0.65	0.67	0.71	0.71	0.65	0.67	0.63
fully open	BC vs L^{-1}	ADP	0.61	0.32	0.6	0.31	0.58	0.33	0.54	0.37
		ATP	0.59	0.32	0.54	0.31	0.64	0.33	0.52	0.35
		apo	0.58	0.32	0.62	0.33	0.61	0.37	0.56	0.37
	BC vs $RMSF^{-1}$	ADP	0.22	0.25	0.46	0.20	0.58	0.29	0.25	0.31
		ATP	0.54	0.33	0.31	0.32	0.59	0.38	0.29	0.33
		apo	0.52	0.40	0.45	0.35	0.45	0.56	0.35	0.44
	RMSF vs L	ADP	0.53	0.89	0.79	0.91	0.91	0.96	0.67	0.97
		ATP	0.95	0.93	0.64	0.95	0.85	0.96	0.61	0.95
		apo	0.89	0.86	0.76	0.93	0.88	0.80	0.77	0.86

[a]N-terminal (NTD), M-domain (MD), and C-terminal (CTD).

destabilize this region, which triggers a conformational shift to the open sate.

Looking at the listed residues in the M-domains of both conformations, phosphorylation of Y313 has been shown to promote Aha1 binding affinity by inducing structural rearrangements that favor cochaperone binding.[93] Residues V368−I370 have been previously identified as key interdomain contacts in a comprehensive network analysis of yeast Hsp90 (V348−I350).[42] Of these residues, the F369A mutation in yeast has been found to drastically decrease ATPase activity by disrupting the positioning of the catalytic R400 which in turn leads to destabilization of the ATP-lid.[16,30,94] Residues L396−L409, listed in the closed but not the open complexes, represent the M-domain catalytic loop where they are thought to form an important interdomain hinge between the NTD and M-domain.[39,95] In addition to the this, S399,[76] R400,[16] E401,[96] and Q404[16] have been implicated in modulating ATPase activity and signal propagation.[34,42] The aromatic cluster formed by F384 and F441 are listed by BC in both conformations and are thought to be important as allosteric control points for nucleotide dependent conformational change, acting as a mechanical hinge between the M- and CTDs.[39,95] Reside E451 is also selected in both conformations and mutation studies have shown that E451A decreases interprotomer interactions leading to decreased ATPase activity,[95] while E451K is thought to perturb the M-domain structure impacting gluticoid receptor binding.[97] Phosphorylation mimicking mutations to S505 is fatal for yeast viability (S485) and is thought to impart resistance to ATP induced conformational transition to the closed state, favoring the open state.[76] Here, S505 is only selected in the open complexes suggesting an important role in this conformation, possibly as a post-translation modification site for regulating the closing transition. Residues E527, Y528, and Q531 have been shown to form part of an important region for client binding in both yeast and *E. coli* Hsp90s[98] and have also been implicated in allosteric regulation,[44] while T545I mutation has been shown to decrease client binding in *E. coli*.[97]

In the CTD, BC lists several prominent peaks in both conformations: The C598-T601 peak includes C598 which has been heavily implicated as a crucial allosteric switch, capable of regulating ATPase cycle.[34,75] Peak T607−L619 in the open conformation corresponds to $helix_{18}$ at the CTD interface. In the closed conformation this peak is extended to include residues W606−K632 representing a coiled loop $helix_{18-19}$. Of these residues: W606 is thought to be involved in client binding and chaperone activity;[98] phosphorylation mimicking mutations to S623 and M625 affect intersubunit communication leading to decreased ATPase rates in yeast;[76] while phosphorylation of Y627 is thought to induce structural rearrangements that reduce the binding affinity of Aha1.[93] Finally, several residues at the four helix bundle ($helix_{21-22}$) located at the extreme C-terminal dimerization site are selected in both conformations. Included in this peak is D680 which has been shown to play an important role in maintaining interprotomer contacts,[95] while several residues from this site in yeast Hsp90 have been reported to participate in fast communication with residues in the NTD,[34] suggesting a nucleotide sensitive regulatory role.

In summary, BC selects several groups of residues in both the closed and FO structures regardless of bound nucleotide, suggesting key intra- and interprotomer communication points. These residues correspond largely to stable regions of the protein and overlap with known functional sites several of which are implicated in conformational dynamics. Furthermore, BC also lists additional residues in regions of as yet unknown function.

BC and L_i are Related to Residue Fluctuations. In this study, BC and L_i were calculated over the course of MD trajectories to make allowance for the potential effect protein dynamics may have on the respective network measures. Thus, far, we have discussed how global domain restructuring in response to bound nucleotide impacts the change in reachability in both the closed and FO complexes (Figure 6 and Figure 7). In this section, we focus on the relative impact local dynamics may have on BC and L_i. Residue fluctuation (RMSF) is a primary example of local dynamics, in which select sites on

DOI: 10.1021/acs.jcim.7b00630
J. Chem. Inf. Model. 2018, 58, 383−404

the protein experience conformational variance relative to the global structure. Structural repositioning of flexible residues is expected to influence the local network by breaking previously established connections between neighbors and/or forming new ones altogether, causing shifts in the local networks that are likely to impact BC and L_i. To assess these assumptions, we take RMSF as an appropriate measure of residue fluctuation and compare its relationship to BC and L_i respectively (Figure 10, Table 3).

In the case of L_i, residues that experience minor fluctuations over the MD trajectory are likely to experience increased connectivity and thus shorter average path lengths, while highly mobile sites are expected to experience lower, more intermittent connectivity and thus longer average path lengths. In this manner, RMSF and L_i could be seen as being proportional to each other, an observation that has been previously reported for protein X-ray structures without molecular dynamics data.[58] Indeed, inspection of the plots in Figure 10 reveals a similar trend between L_i and RMSF for both conformations, particularly for peak regions. However, comparison of these two metrics using the Pearson's correlation coefficient indicates much higher correlations for the FO complexes compared to the closed complexes (Table 3). This observation can be explained by the relative plasticity of the two structures at equilibrium. As previously discussed and shown in this study, the closed conformation is the most stable form of the protein compared to the FO conformation which is significantly more flexible. Comparison of their respective RMSF plots reveals on average higher fluctuations for the FO complexes compared to the closed complexes (Figure S3 and Figure S9). This difference in distance fluctuation is significant in that the underlying local network graphs are likely to be more severely impacted by large distance fluctuations which may cause the distance between connected residues to exceed the 6.7 Å distance cutoff,[79] and in doing so reduce the degree of connectivity within the local networks when averaged over the whole trajectory. For the FO complexes, the NTDs and M-domains of both protomers experience increased RMSF compared to the CTD which is more stable due to its involvement as the primary interprotomer dimerization site and comparison of the correlation coefficients for these domains reveals larger values for NTDs and M-domains. Conversely, in more stable structures such as the closed complexes, the likelihood of residue fluctuations affecting path length is decreased due to the inherent rigidity of the structure, where the magnitude of the fluctuations may be insufficient to exceed the 6.7 Å distance cutoff. In this scenario, previously established connectivity between neighboring residues would remain intact despite minor local residue fluctuations, causing the trend between L_i and RMSF to deviate and negatively impact the correlation coefficient. An example of this is observed when comparing the correlation coefficients for the closed conformations which show subtle differences between the different nucleotide configurations. Therein, the apo form records slightly higher correlation coefficients compared to the ATP and ADP configurations (Table 3). This observation supports the aforementioned proportional relationship between L_i and RMSF, in that the apo complex which engenders a higher degree of flexibility compared to the nucleotide bound complexes (see previous sections), records slightly larger residue fluctuations (Figure S3), and thus a stronger correlation with L_i. In addition to local fluctuations, we note that the degree of compactness of the network graph could also be a contributing factor to minor deviations between RMSF and L_i. For example, the closed conformation complexes (and the CTDs of the FO complexes) have more compact local networks due to their 3D structural arrangements, and are thus afforded a greater number of possible paths to navigate the network. This increased selection of possible routes may enable L_i to utilize alternate routes to avoid local fluctuations, thus allowing L_i to remain fairly stable compared to RMSF. We test these hypotheses on the FO ATP complex by comparing the RMSF with different L_i calculated based on several distance cutoffs (6.7, 9.0, and 12.0 Å) (Figure S11A). In this analysis, the correlation between L_i and RMSF is seen to hold for the flexible NTDs and M-domains regardless of cutoff but decreases severely (up to 3-fold) for the more compact rigid CTDs as the cutoff increases (Figure S11A labels), demonstrating how the potential effect of RMSF on local network arrangements decreases when the magnitude of the fluctuations is close to or less than the specified distance cutoff. These observations are in agreement with a previous study that demonstrates how increased cutoffs (>8.5 Å) cause L_i to gradually converge toward the theoretical limit.[58]

In summary, we suggest that L_i and RMSF share a proportional relationship, and that deviation from this trend may arise when residue fluctuations are of an insufficient magnitude to affect the connectivity of the local network, or when the structure is suitably compact such that alternative routes may be taken to avoid increased L_i in response to fluctuation of the local network. Furthermore, we note that care should be taken when setting the distance cutoff for the construction of the network graph, and note that if the cutoff is too large and the system is predominantly rigid/compact, residue fluctuations will have a reduced effect on the observed local network.

Next, we look at BC, which is intricately coupled to L_i, in that it is a measure of the number of shortest paths that pass through a given node. Here, regions of the protein that record high BC are likely to be structurally stable and experience minor fluctuations, such that they are consistently available as communicating nodes. Based on this assumption, RMSF and L_i could be expected to correlate inversely with respect to BC. This is found to be the case for both conformers in which peak BC regions are seen to be inversely proportional to both L_i and RMSF. Residues with high BC appear to correlate with regions of the protein that experience minor residue fluctuations and shorter L_i (Figure 10 peaks). We note that in both conformations, stronger correlations are observed between L_i and BC than between RMSF and BC (Table 3). This observation could be explained by the aforementioned inferences regarding the relationship between L_i and RMSF, whereby L_i may provide a more accurate description of the local network surrounding high BC regions as it is potentially a more stable quantity compared to RMSF. Furthermore, we note that the Pearson's correlations between BC-RMSF and BC-L_i to be higher for the closed conformation complexes than the open complexes, and suggest this to be a limitation of the Pearson's correlation coefficient, which is more suitable to linear data sets. Nevertheless, good agreement is seen for peak BC regions, which correlate to some degree with local peaks in the RMSF and L_i curves (Figure 10), but not necessarily for non-BC regions. Finally, as with L_i, we examine the effect distance cutoff has on the inverse relationship between BC and RMSF for the ATP bound FO complex (Figure S11 B). In this analysis, increased distance cutoffs appear to have little effect on the

DOI: 10.1021/acs.jcim.7b00630
J. Chem. Inf. Model. 2018, 58, 383−404

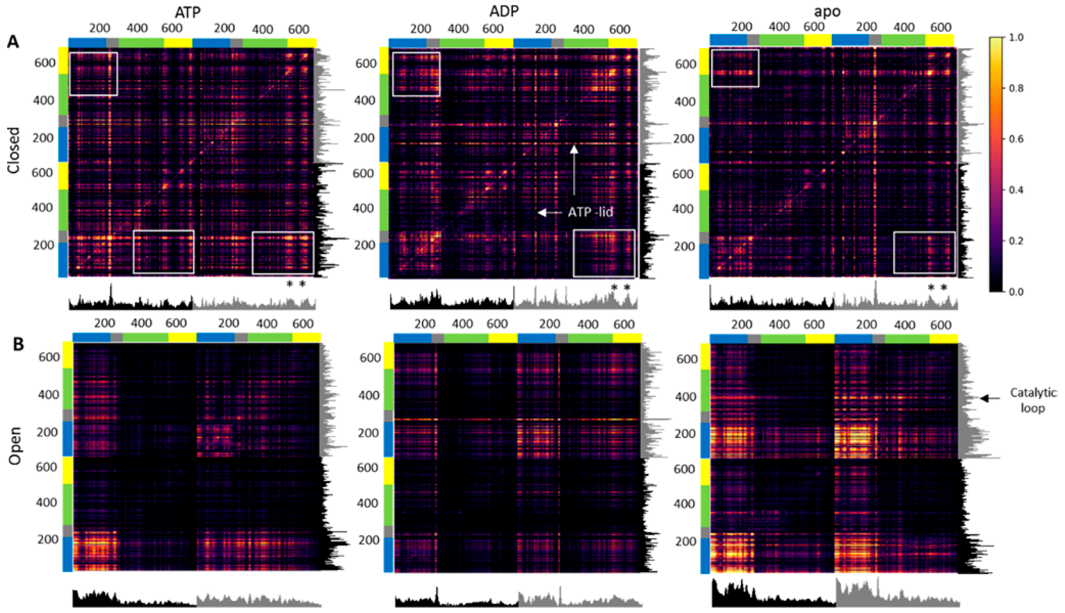

Figure 11. PRS response maps showing effector and sensor regions of the protein: (A) closed and (B) fully open complexes. Columns denote sensor residues, while rows represent effector (perturbed) residues. Bright spots indicate highly sensitive residues that experience large displacements. Accompanying each map are "effector" bar plots on the right-hand-side and at the bottom "sensor" column plots (protomer 1 black, protomer 2 gray) which represent the sum/average of the matrix elements. * symbols denote $helix_{17}$ and $helix_{20}$.

selection of high BC regions, with peak residues remaining consistent over all three distance cutoffs examined (6.7, 9.0, and 12.0 Å). We do however note that the frequency of usage for these peak residues is altered by changing the cutoff, but with no observable trend. For example, residues 501 and 523 have a higher degree of usage in protomer 1 for the 9.0 Å cutoff, compared to the 6.7 and 12.0 Å cutoffs. From a structural perspective, the larger cutoff distances appear to increase BC for flexible regions of the protein, such as $helix_{17}$ and $helix_{18}$ (res 600−630). This observation is likely to arise when the magnitude of the residue fluctuations is insufficient to exceed the cutoff for connected residues thus enabling a higher probability for shortest path navigation via these flexible regions over the course of the MD trajectory. Comparison of the Pearson's correlation coefficient between $RMSF^{-1}$ and BC for each distance cutoff reveals similar correlation coefficients over the three functional domains of the protein. However, we note that the smaller distance cutoffs improve the correlations for the more compact CTDs, likely due to the reduced impact of the flexible $helix_{17}$ and $helix_{18}$ for the larger distance cutoffs.

Overall, we find RMSF and L_i to be largely proportional to one another, but note that this relationship is linked to the magnitude of the distance fluctuations, the distance cutoff used to construct the network graphs, as well as the relative compactness of the local networks. Furthermore, we show for the first time that there exists an inverse relationship between these network measures and BC that holds true even for increased distance cutoffs, and note that L_i may provide a more accurate description of the effect of the local network on function compared to RMSF. These observations were all confirmed for separate replicate trajectories in which similar trends were observed (Table S12). Finally, we propose that since not all residues displaying small fluctuations act as communication bridges, we suggest BC and L_i to be alternative and potentially more sensitive quantities to follow for the identification of novel functional sites on proteins.

Perturbation Response Scanning. PRS is a technique used to assess the allosteric influence each residue has on all other residues when externally perturbed. Several previous studies have demonstrated the use of PRS as an effective approach for the identification of functionally important sites that are potentially involved in modulating binding-region motions,[60−62,99−101] and PRS analysis has been previously shown to be an efficient method for determining the allosteric potential of large multidomain proteins.[62,99] Briefly, PRS uses linear response theory to predict whole protein displacements in response to the insertion of external forces at single residue sites (see eq 4. In this study, 250 perturbations were sequentially applied to each residue in the protein and the resultant displacement of the whole protein in response to each perturbation recorded in a 3D matrix and analyzed in terms of (1) average relative displacement—to gain insight on protein sensitivity to external force perturbation and (2) conformational overlap with a known target state—to assess the potential of each residue to select displacements that are representative of an expected conformational change. Together these analyses provide insight regarding site on the protein that are potentially involved in modulating conformational dynamics.

Average Residue Displacements Identify Putative Allosteric Effector and Sensor Residues. Analysis of the average response of the whole protein to 250 perturbations of each residue allows for the identification of sites on the protein that are allosterically sensitive to external force perturbations. Conversely, residues whose perturbations result in large conformational changes elsewhere in the protein can be seen as allosteric effectors, representing sites on the protein likely involved in external binding events such as specific cochaperone and client binding in the case of Hsp90. This analysis approach for PRS has been previously demonstrated on Hsp70 by General et al.[99] The average displacement response maps for both configurations of the protein are shown in Figure 11, in which the *ik*th entry refers to the average response (displace-

DOI: 10.1021/acs.jcim.7b00630
J. Chem. Inf. Model. 2018, 58, 383−404

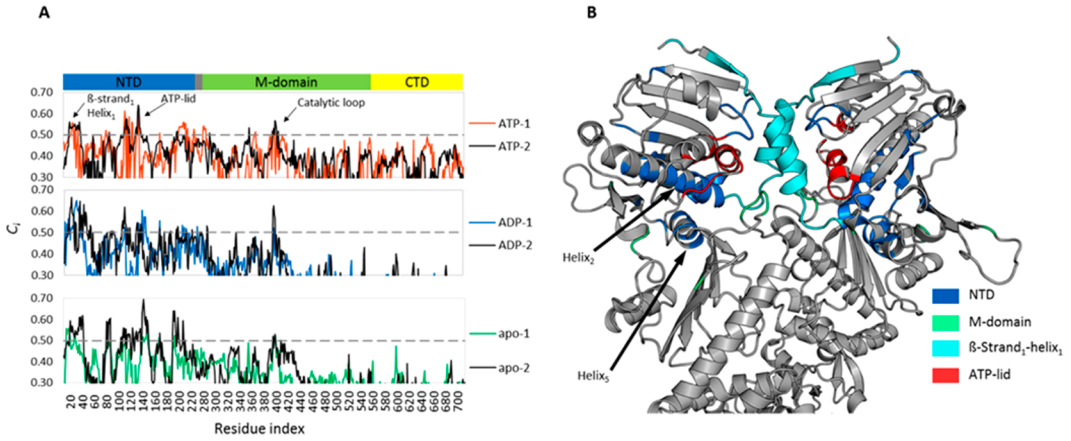

Figure 12. Residues accentuated by PRS in the closed conformation complexes. (A) PRS profiles showing accentuated residues which select the open conformation. Protomer 1 is colored by NTD configuration (ATP red, ADP blue, apo green), and protomer 2 in black. (B) Zoomed in view of the NTD of the closed conformation, showing the accentuation of the NTD dimerization interface of the ADP bound complex. Residues accentuated by PRS are colored according to domain location.

ment) of residue k to external perturbation at residue i. Thus, bright spots indicate peak residues that experience large displacements, while darker areas imply residues that experience little or no displacement. Accompanying each map, are the most influential "effector" residues (rows) in the right-hand bar plots, and the most sensitive "sensor" residues (columns) in the lower column plots.

For the closed conformation complexes (Figure 11A), comparing the displacement intensities of the different NTD configurations reveals the ADP complex to be the most sensitive to external force perturbations, while the apo complex appears to be the least sensitive. This observation may suggest that the ADP closed complex is more amenable to conformational change compared to the other configurations, in agreement with the hypothesis that ADP imparts protomer flexibility. Strong sensor and effector signals are recorded at the linker regions of all three complexes. These residues correspond to the G−G−G−G insert, introduced in the homology modeling process to cover the missing linker region (see Methodology), and their high degree of displacement is to be expected as glycine residues are known to be highly mobile elements. Several sensor peaks are observed in all three closed configuration complexes: ß-strand$_1$ (res 15−20); helix$_1$ (res 21−36); the first turn of the NTD ß-sheet (res 81−88); the ATP-lid (res 120−129); ß-strand$_4$ (res 170−180); the loop connecting helix$_{12}$ and helix$_{13}$ (res 469−472); as well as helix$_{17}$ (res 550−590) and helix$_{20}$ (res 638−660) in the CTD. Nucleotide dependent differences are also observed for residues that correspond to Aha1 binding (res 300−308),[102] the catalytic loop and interdomain hinge[39] (res 391−406), the phosphorylation site Y313,[93] helix$_{13}$ (res 478−490), and the putative client binding site at helix$_{16}$ (res 523−530) experience increased sensitivity in the presence of ADP, but not the ATP and apo complexes. Studying the corresponding effector sites, interprotomer coupling is observed between the NTD and CTD in all three complexes, where perturbations at the CTD (helix$_{17}$ and helix$_{20}$) of protomer 2 are strongly detected at the NTD of protomer 1 and *vice versa* (Figure 11A, white boxes). For the ATP complex, NTD perturbations in protomer 1 appear to illicit a stronger CTD response in both protomers compared to the ADP and apo complexes, while CTD perturbations in protomer 2 of the ADP and apo complexes appear to illicit a stronger response at the NTD of protomer 1 compared to the ATP complex. This observed allosteric coupling between the two terminals is in agreement with a previous computational study demonstrating efficient allosteric communication between the NTD and CTD in response to bound nucleotide.[34] Other notable effector residues include the ATP-lid (res 121−126), particularly in the ADP bound complex, helix$_{10}$ (res 406−425), and residues surrounding A469 and G515 in the M-domain. These sites are significant in that ATP-lid stabilization is necessary to maintain the closed "active" state, while helix$_{10}$ has been implicated in allosteric signal propagation between the NTD and M-domain in HtpG.[40] Furthermore, all of the M-domain sites are located on the surface of the protein, in positions easily accessible to cofactor binding.

The open conformation complexes (Figure 11B) show clear differentiation between the different complex configurations. However, all three complexes show strong allosteric coupling between their NTDs, where perturbations at the NTD of one protomer lead to strong displacement signals at NTD of the second protomer. Interestingly, the apo complex appears to be the most sensitive to NTD perturbations while the ATP complex appears to be more sensitive than ADP. This observation suggests the apo complex to be more amenable to conformational change, an observation that is in agreement with previous reports describing stochastic conformational dynamics for apo Hsp90.[74,77,78] Looking in more detail, it is also apparent that perturbations arriving at the NTD result in displacements at the M- and CTD depending on the nucleotide configuration. M-domain displacements at ß-turn E332-E336 and the catalytic loop (res 395−407) are observed within the perturbed protomer of the ATP and apo complexes, while CTD sensitivity at helix$_{17}$ (552−570) is observed for the ADP complexes. Interestingly, most of these nucleotide specific sensor sites are also listed as allosteric effectors for the respective complexes, implying allosteric coupling between these sites.

Perturbation of Key Residues Reveals Sites Likely Involved in Modulating Conformational Change. In this section, PRS is used to identify residues whose perturbation invoke a conformational change toward an expected target conformation representative of the opposite state. For each residue, the displacement response for each sequential perturbation is compared to a known experimental displacement (opening or

DOI: 10.1021/acs.jcim.7b00630
J. Chem. Inf. Model. 2018, 58, 383−404

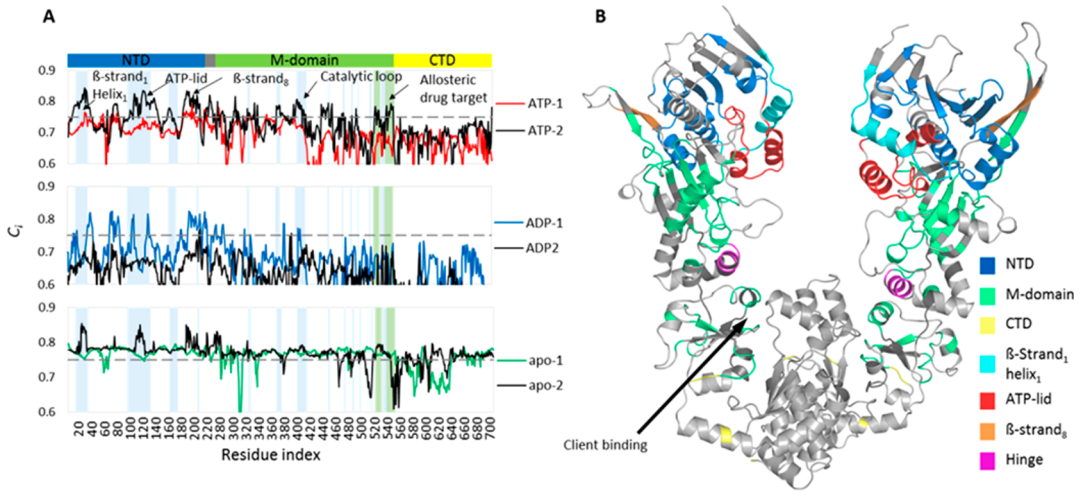

Figure 13. Residues accentuated by PRS in the open conformation complexes. (A) PRS profiles showing accentuated residues capable of selecting the closed conformation. Protomer 1 is colored by NTD configuration (ATP red, ADP blue, apo green), and protomer 2 in black. Blue shading represents overlap with Aha1 binding residues and the green shading client binding residues. (B) Structural mapping of residues accentuated by PRS for the FO-ATP complex colored by location.

closing), and the goodness of fit measured using the Pearson's correlation coefficient (eq 5). In this manner, each residue records 250 correlation coefficients, and the highest correlation, C_i, is selected to represent the maximum potential for that residue to invoke a conformational change toward the opposite state. The closed complexes are assessed in terms of the opening transition, and the FO complexes in terms of the closing transition, and the results of these analyses shown in Figures 12 and 13, respectively. To ensure reproducibility of this technique for large flexible systems such as Hsp90, duplicate PRS calculations for each complex were calculated from separate MD trajectories and report good overlap for peak residues (Figure S13). The highest C_i residues are summarized in Table S14, and their relative functional importance is discussed in more detail bellow.

For the closed conformation complexes (Figure 12A), PRS indicates that regardless of bound nucleotide, no single residue is capable of selecting the open conformation in response to external force perturbation, with peak residues recording maximum C_i values of ∼0.60. Despite this, several C_i residue peaks (C_i > 0.50) appear to correspond to functional sites previously identified and discussed in the BC analysis. Accentuated residues belonging to ß-strand$_1$ (res 16, 19, 20); helix$_1$ (res 23−40); the ATP-lid (res 107−113, 116, 119, 130−132, 134, 135, 137−139, 142−145); and the catalytic loop (res 397−400) form a central dimerization hub at the NTD and have been previously described as forming part of an NTD/M-domain mechanical hinge[39] (Figure 12B). Destabilization of these interprotomer interfaces is crucial before protomer uncoupling and a conformational shift to the open state can occur.[90] PRS also accentuates residues residing in helix$_2$ (res 41−65); ß-strand$_2$ (res 88−94); helix$_5$ (res 203, 205, 209−211); and ß-strand$_8$ (214, 219). Of these, helix$_2$ has been previously reported to play a crucial role in propagating allosteric signals from the NTD to the M-domain in *E. coli* Hsp90,[40] while residues residing in ß-stand$_2$ have been associated with long-range communication with the CTD.[34] The NTD/linker interface formed by helix$_5$ and ß-strand$_8$ has been implicated in modulating chaperone affinity[20] and conformational transitions in response to bound nucleotide.[92] Comparing the highest C_i between complexes, residues belonging to the ATP-lid recorded the highest C_i values in the ATP and apo complexes (0.62 and 0.67 respectively), while residues belonging to ß-strand$_1$, helix$_1$, and the catalytic loop recorded the highest C_i values for the ADP complex.

Studying the open complexes, the nucleotide configuration appears to have a marked differential effect on the potential of each complex to interconvert to the closed state. Comparing the percentage of residues with C_i > 0.75, the ATP (33%) and ADP (11%) complexes record far fewer than the apo complex (85%). The elevated number of C_i > 0.75 in the apo complex is interpreted to be indicative of a natural propensity for this complex to interconvert to the closed state, an observation in keeping with the hypothesis that the apo protein behaves stochastically.[74,77,78] In the case of the nucleotide bound complexes, PRS only lists select residues capable of eliciting a conformational transition toward the closed state.

Looking at the C_i profile for the ATP bound complex (Figure 13A), PRS accentuates several residue clusters in the NTD and M-domain (Figure 13A, peaks) which once again point to functionally important regions. In the NTD, these residues include: ß-strand$_1$ (res 20−24); helix$_1$ (res 25−35); helix$_2$ (res 43−53); the ATP-lid (res 113−136); ß-strand$_5$ (res 163−170, 173−174); ß-strand$_6$ (res 186−190); helix$_{6-7}$ (res 191−214); and ß-strand$_8$ (res 219−224), and in the M-domain: helix$_9$ (res 312−316); several residues belonging to the ß-sheet (res 319, 320, 326, 330−338, 341, 343, 347, 360, 361, 363, 376−393); the catalytic loop (res 402−410); helix$_{10}$ (res 411, 412, 416−418, 420); helix$_{12}$ (res 443−449, 451−454); helix$_{16}$ (res 523−525, 527, 529, 530); and last loop residues T540−L551. Of these accentuated sites, the functional importance of ß-strand$_1$, helix$_{1-2}$, ß-strand$_8$, the ATP-lid, and the catalytic loop have already been discussed in context of the opening transition; however, accentuation of these elements by PRS for the FO-ATP complex, and thus the closing transition, also bears functional significance. It is widely believed that ATP binding initiates the closing transition by triggering the uncoupling of the ß-strand$_1$ and helix$_1$ from the ATP-lid, leading to its release and closure over the nucleotide binding pocket. This conformational repositioning of the ATP-lid not only entraps bound nucleotide, but also facilitates N-terminal dimerization through exposure of a hydrophobic surface required for ß-

DOI: 10.1021/acs.jcim.7b00630
J. Chem. Inf. Model. 2018, 58, 383−404

strand$_1$ swapping and stabilization of the closed active complex.[90] In addition to these NTD conformational dynamics, ATPase activation of the closed complex is only fully achieved when the M-domains dock onto their respective NTDs, allowing the M-domain catalytic loop to be repositioned such that R400 projects into the nucleotide binding pocket to coordinate with the γ-phosphate of ATP.[16,26] Interestingly, we note that PRS accentuates ß-strand$_1$, helix$_1$, and the ATP-lid in the FO-ATP complex, but not in the FO-ADP complex (Figure 13A), a finding that supports the hypothesis that ATP binding allosterically activates the closing transition, while bound ADP stabilizes the open conformation. The conformational dynamics required for ATPase activation in Hsp90 are thought to be the rate limiting step in an inherently slow process, recording rate constants in the order of minutes.[15,27,28,103] Indeed, a recent study has linked the rate constant of ATP hydrolysis with the rate constants of ATP-lid closure, ß-strand swapping, and intraprotomer association of the NTD and M-domains.[30] Furthermore, the authors of this study propose a two-step mechanism for ATP-lid closure and find evidence of a previously unknown mode of action for the cochaperone Aha1, where they suggest its involvement in facilitating early mobilization of the ATP-lid.[30] Here, we find that residues accentuated by PRS in the ATP complex are clustered around NTD and M-domain sites that have been previously implicated in Aha1 binding[16,104] (Figure 13A, blue shading). We propose that perturbations arriving at ß-strand$_1$, helix$_1$, and the ATP-lid may occur naturally through binding interactions with Aha1, providing possible evidence in support of Aha1 assisted ATP-lid closure and interstate conversion to the closed state. Also of functional importance and accentuated by PRS in the ATP complex, are residues belonging to helix$_{12}$ corresponding to the M-domain/CTD hinge,[39,42] as well as helix$_{16}$ and loop T540-L551 which are thought to be important regulatory sites for client binding[42,97,98] (Figure 13A, green shading). Interestingly, this CTD region has been previously reported to be an allosteric drug target site,[36] and subsequent drug discovery studies have demonstrated how bound ligands at this site can allosterically enhance ATPase activity through the asymmetric modulation of protomer conformational dynamics.[37,105]

Overall, the data presented here suggests PRS to be a suitable technique for identifying cofactor binding sites that may be specifically involved in allosteric modulation of conformational dynamics. To tests this hypothesis, we analyzed the PRS data for the FO-ATP complex in terms of sites known to be involved in binding interactions with the heat shock organizing protein (HOP) (res: E307, E311, K314, N318, W320, D322, K431, E432, E473, A469, T482, and E486).[106,107] HOP is thought to modulate Hsp90's conformational dynamics by interrupting NTD dimerization through steric interference rather than allosteric mechanisms[6] and thus presents as a suitable negative control. With the exception of K314 and W320, PRS does not accentuate the HOP binding residues in the FO-ATP, confirming that cofactor binding residues identified by PRS are likely allosteric modulators of conformational dynamics.

CONCLUSIONS

To date, numerous biochemical and computational studies have made considerable advances toward understanding how Hsp90 modulates its complex conformational cycle. In this study, we have assessed the current opinions regarding Hsp90's conformational dynamics, with respect to the human Hsp90α isoform, in a comprehensive analysis of full length homology models of the human Hsp90α, using all-atom MD simulations coupled with in depth DRN analysis and PRS techniques.

Within the limitations of all-atom MD simulations, our results are in agreement with previous studies describing a differential effect of bound nucleotide on conformational dynamics in which ATP drives NTD dimerization and the closing transition, while the ADP/apo complexes favor the open Hsp90 dimer.[17,23,24,74,108] Regardless of the conformation, bound ATP was found to tense the dimer complex in favor of the closed conformation, while ADP appeared to relax the protomers affording a greater degree of flexibility. Bound ADP in the partially open complex increased protomer flexibility, resulting in global conformational rearrangements representing the opening transition and the fully open client loading conformation.[23−25] Analysis of the change in residue reachability over time confirmed the "tensing" and "relaxing" effect of ATP and ADP respectively, with notable reduction in average path length in the former, and variable increased path lengths in the latter. Locations in the protein recording large changes in reachability corresponded to key functional elements such as ß-strand$_1$, helix$_1$, ATP-lid, and catalytic loop, implicating these regions in steering conformational dynamics. Betweenness centrality analysis provided a measure for distinguishing sites in the protein responsible for intraprotein communication. These sites were found to correlate closely with known functional sites, demonstrating how BC analysis may be used to identify functional sites on a protein.

PRS was used to probe both the closed and open conformation complexes, to assess each residue's allosteric potential to affect conformational changes. Analysis of the average response of the whole protein to external force perturbation revealed an interprotomer allosteric coupling between the NTD and CTD of the closed complexes, in which perturbations arriving at the terminal end of one protomer are felt or "sensed" at the opposite terminal of the other protomer. This observation is in agreement with a recent study demonstrating efficient communication between the two domains, leading to the discovery of a CTD allosteric drug target site.[34,36,75,109] In a similar manner, analysis of the open complexes demonstrated allosteric coupling between the NTDs of each protomer, the apo complex showing particular sensitivity to perturbations at the NTDs, and an increased sensitivity of the ATP complex over the ADP complex, suggesting ATP driven allosteric activation of this complex. It is well documented that regulation of Hsp90's conformational cycle is largely impacted by various cochaperone interactions.[6,73,74] The perturbations utilized in PRS provide a novel way of introducing external influences on select residues that could be likened to the natural forces involved in cofactor and client binding. PRS analysis of the closed complexes revealed no single residue perturbations capable of selecting a coordinate change toward the open conformational state. It is thus likely that the opening transition occurs spontaneously without the aid of external binding partners. Interestingly, the highest C_i residues selected by PRS for the closed complexes include residues that make up the primary NTD dimerization site, including ß-strand$_1$, helix$_1$, ATP-lid, and M-domain catalytic loop, elements that have been previously reported to form an important NTD/M-domain hinge implicated in conformational dynamics.[39] Unlike the closed complexes, PRS analysis of the open conformation complexes revealed several sites in the NTD and M-domain capable of selecting a conformational

DOI: 10.1021/acs.jcim.7b00630
J. Chem. Inf. Model. 2018, 58, 383−404

change toward the closed form. Most of the residues at these sites also correlate to known functional sites, while several map to regions on the surface of the protein believed to be cochaperone binding sites[6] (Figure 14). In particular, PRS

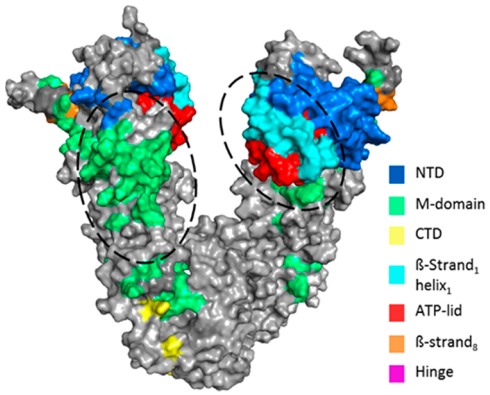

Figure 14. Surface representation of Hsp90 depicting PRS hot spots capable of selecting a conformational change toward the closed complex. Ellipses denote regions that overlap with known cofactor binding sites.

accentuates a number of residues in the ß-strand$_1$, helix$_1$, ATP-lid, and catalytic loop regions of the FO-ATP complex. These residues correspond with sites implicated in Aha1 binding interactions, suggesting that perturbations at these sites may arrive naturally through cochaperone binding interactions. This hypothesis is in keeping with recent reports implicating Aha1 in early ATP-lid mobilization,[30] acceleration of ATPase activation,[96] and allosteric modulation of Hsp90's conformational dynamics.[43] The accentuation of these residues in the FO-ATP but not the FO-ADP complex reinforces the hypothesis that ATP allosterically activates or primes the open complex for conformational transition toward the closed state.

In summary, this study demonstrated how all atom MD simulations coupled with dynamic network analysis and PRS can be used to gain further insights regarding allosteric regulation of conformational dynamics in large complex proteins such as human Hsp90α. Collectively, these methods provide a computationally feasible platform to determine functional residues implicated in modulating conformational dynamics, offering routes for novel rational experimental investigations on chaperone function and allosteric regulation.

■ ASSOCIATED CONTENT

Supporting Information

The Supporting Information is available free of charge on the ACS Publications website at DOI: 10.1021/acs.jcim.7b00630.

Table S1 comparison of best scoring homology models before and after energy minimization; Figure S2 comparative RMSD plots of the replicate trajectories for the (A) closed and (B) fully open conformation complexes; Figure S3 RMSF plots of closed conformation complexes; Figure S4 final closed conformation structures after 100 ns MD simulations for ATP (red); ADP (blue); and apo (green); Figure S5 comparison of replicate DCC heat maps for the (A) closed and (B) fully open conformation complexes; Figure S6 (A) final structures of the partially open complexes after 200 ns MD simulations; (B) bacterial HtpG structure (PDB 2IOQ) (cyan) superimposed on the 200 ns ADP complex structure (gray); Figure S7 RMSF plots of the partially open complexes; Figure S8 (A) RMSD and (B) NTD interprotomer distance plots for the fully open complexes; Figure S9 RMSF plots for the fully open complexes; Figure S10 comparative ΔL_i plots for the replicate trajectories for the (A) closed and (B) fully open conformation complexes; Figure S11 comparison of (A) RMSF vs L_i and (B) 1/RMSF vs BC for several network graphs constructed based on different distance cutoffs (6.7, 9.0, and 12.0 Å); Table S12 comparison of BC/ΔL_i^{-1}/RMSF^{-1} by Pearson's correlation coefficient, for each separate replicate trajectories NTD, MD, and CTD; Figure S13 comparative PRS profiles for separate MD trajectories for the (A) closed and (B) the fully open conformation complexes; Table S14 summary list of residues accentuated by PRS for the closed (C_i > 0.50) and open (C_i > 0.75) complexes (PDF)

■ AUTHOR INFORMATION

Corresponding Author

*E-mail: O.TastanBishop@ru.ac.za.

ORCID

Canan Atilgan: 0000-0003-0557-6044

Özlem Tastan Bishop: 0000-0001-6861-7849

Funding

This work is supported by the National Research Foundation (NRF) South Africa (Grant Number 93690) and the Scientific and Technological Research Council of Turkey (Grant Number 116F229). The content of this publication is solely the responsibility of the authors and does not necessarily represent the official views of the funders.

Notes

The authors declare no competing financial interest.

■ ACKNOWLEDGMENTS

The authors thank the Centre for High Performance Computing (CHPC), South Africa, for computing resources. The authors thank the manuscript reviewer who suggested a comparative analysis of BC and RMSF.

■ REFERENCES

(1) Taipale, M.; Jarosz, D. F.; Lindquist, S. HSP90 at the Hub of Protein Homeostasis: Emerging Mechanistic Insights. *Nat. Rev. Mol. Cell Biol.* **2010**, *11*, 515−528.

(2) Young, J. C.; Moarefi, I.; Hartl, F. U. Hsp90: A Specialized but Essential Protein-Folding Tool. *J. Cell Biol.* **2001**, *154*, 267−273.

(3) McClellan, A. J.; Xia, Y.; Deutschbauer, A. M.; Davis, R. W.; Gerstein, M.; Frydman, J. Diverse Cellular Functions of the Hsp90 Molecular Chaperone Uncovered Using Systems Approaches. *Cell* **2007**, *131*, 121−135.

(4) Zhao, R.; Davey, M.; Hsu, Y.-C.; Kaplanek, P.; Tong, A.; Parsons, A. B.; Krogan, N.; Cagney, G.; Mai, D.; Houry, W. A.; et al. Navigating the Chaperone Network: An Integrative Map of Physical and Genetic Interactions Mediated by the Hsp90 Chaperone. *Cell* **2005**, *120*, 715−727.

(5) Pearl, L. H.; Prodromou, C. Structure and Mechanism of the Hsp90 Molecular Chaperone Machinery. *Annu. Rev. Biochem.* **2006**, *75*, 271−294.

(6) Schopf, F. H.; Biebl, M. M.; Buchner, J. The HSP90 Chaperone Machinery. *Nat. Rev. Mol. Cell Biol.* **2017**, *18*, 345−360.

(7) Friedman, D. Pseudotumor Cerebri. *Neurol. Clin.* **2004**, *22*, 99−131.

(8) Jhaveri, K.; Taldone, T.; Modi, S.; Chiosis, G. Advances in the Clinical Development of Heat Shock Protein 90 (Hsp90) Inhibitors in Cancers. *Biochim. Biophys. Acta, Mol. Cell Res.* **2012**, *1823*, 742−755.
(9) Taldone, T.; Ochiana, S. O.; Patel, P. D.; Chiosis, G. Selective Targeting of the Stress Chaperome as a Therapeutic Strategy. *Trends Pharmacol. Sci.* **2014**, *35*, 592−603.
(10) Pallavi, R.; Roy, N.; Nageshan, R. K.; Talukdar, P.; Pavithra, S. R.; Reddy, R.; Venketesh, S.; Kumar, R.; Gupta, A. K.; Tatu, U.; et al. Heat Shock Protein 90 as a Drug Target against Protozoan Infections. *J. Biol. Chem.* **2010**, *285*, 37964−37975.
(11) Roy, N.; Nageshan, R. K.; Ranade, S.; Tatu, U. Heat Shock Protein 90 from Neglected Protozoan Parasites. *Biochim. Biophys. Acta, Mol. Cell Res.* **2012**, *1823*, 707−711.
(12) Faya, N.; Penkler, D. L.; Tastan Bishop, Ö. Human, Vector and Parasite Hsp90 Proteins: A Comparative Bioinformatics Analysis. *FEBS Open Bio* **2015**, *5*, 916−927.
(13) Wayne, N.; Bolon, D. N. Dimerization of Hsp90 Is Required for in Vivo Function. Design and Analysis of Monomers and Dimers. *J. Biol. Chem.* **2007**, *282*, 35386−35395.
(14) Mayer, M. P.; Le Breton, L. Hsp90: Breaking the Symmetry. *Mol. Cell* **2015**, *58*, 8−20.
(15) Prodromou, C.; Roe, S. M.; O'Brien, R.; Ladbury, J. E.; Piper, P. W.; Pearl, L. H. Identification and Structural Characterization of the ATP/ADP-Binding Site in the Hsp90 Molecular Chaperone. *Cell* **1997**, *90*, 65−75.
(16) Meyer, P.; Prodromou, C.; Hu, B.; Vaughan, C.; Roe, S. M.; Panaretou, B.; Piper, P. W.; Pearl, L. H. Structural and Functional Analysis of the Middle Segment of Hsp90: Implications for ATP Hydrolysis and Client Protein and Cochaperone Interactions. *Mol. Cell* **2003**, *11*, 647−658.
(17) Ali, M. M. U.; Roe, S. M.; Vaughan, C. K.; Meyer, P.; Panaretou, B.; Piper, P. W.; Prodromou, C.; Pearl, L. H. Crystal Structure of an Hsp90-Nucleotide-p23/Sba1 Closed Chaperone Complex. *Nature* **2006**, *440*, 1013−1017.
(18) Harris, S.; Shiau, A.; Agard, D. The Crystal Structure of the Carboxy- Terminal Dimerization Domain of htpG, the Escherichia Coli Hsp90, Reveals a Potential Substrate Binding Site. *Structure* **2004**, *12*, 1087−1097.
(19) Hainzl, O.; Lapina, M. C.; Buchner, J.; Richter, K. The Charged Linker Region Is an Important Regulator of Hsp90 Function. *J. Biol. Chem.* **2009**, *284*, 22559−22567.
(20) Tsutsumi, S.; Mollapour, M.; Graf, C.; Lee, C.-T.; Scroggins, B. T.; Xu, W.; Haslerova, L.; Hessling, M.; Konstantinova, A. A.; Neckers, L.; et al. Hsp90 Charged-Linker Truncation Reverses the Functional Consequences of Weakened Hydrophobic Contacts in the N Domain. *Nat. Struct. Mol. Biol.* **2009**, *16*, 1141−1147.
(21) Tsutsumi, S.; Mollapour, M.; Prodromou, C.; Lee, C.-T.; Panaretou, B.; Yoshida, S.; Mayer, M. P.; Neckers, L. M. Charged Linker Sequence Modulates Eukaryotic Heat Shock Protein 90 (Hsp90) Chaperone Activity. *Proc. Natl. Acad. Sci. U. S. A.* **2012**, *109*, 2937−2942.
(22) Jahn, M.; Rehn, A.; Pelz, B.; Hellenkamp, B.; Richter, K.; Rief, M.; Buchner, J.; Hugel, T. The Charged Linker of the Molecular Chaperone Hsp90 Modulates Domain Contacts and Biological Function. *Proc. Natl. Acad. Sci. U. S. A.* **2014**, *111*, 17881−17886.
(23) Shiau, A. K.; Harris, S. F.; Southworth, D. R.; Agard, D. a. Structural Analysis of E. Coli hsp90 Reveals Dramatic Nucleotide-Dependent Conformational Rearrangements. *Cell* **2006**, *127*, 329−340.
(24) Dollins, D. E.; Warren, J. J.; Immormino, R. M.; Gewirth, D. T. Structures of GRP94-Nucleotide Complexes Reveal Mechanistic Differences between the hsp90 Chaperones. *Mol. Cell* **2007**, *28*, 41−56.
(25) Southworth, D. R.; Agard, D. a. Client-Loading Conformation of the Hsp90 Molecular Chaperone Revealed in the Cryo-EM Structure of the Human Hsp90:Hop Complex. *Mol. Cell* **2011**, *42*, 771−781.
(26) Prodromou, C. The "Active Life" of Hsp90 Complexes. *Biochim. Biophys. Acta, Mol. Cell Res.* **2012**, *1823*, 614−623.
(27) Scheibel, T.; Neuhofen, S.; Weikl, T.; Mayr, C.; Reinstein, J.; Vogel, P. D.; Buchner, J. ATP-Binding Properties of Human Hsp90. *J. Biol. Chem.* **1997**, *272*, 18608−18613.
(28) McLaughlin, S. H.; Smith, H. W.; Jackson, S. E. Stimulation of the Weak ATPase Activity of Human hsp90 by a Client Protein. *J. Mol. Biol.* **2002**, *315*, 787−798.
(29) Hellenkamp, B.; Wortmann, P.; Kandzia, F.; Zacharias, M.; Hugel, T. Multidomain Structure and Correlated Dynamics Determined by Self-Consistent FRET Networks. *Nat. Methods* **2017**, *14*, 174−180.
(30) Schulze, A.; Beliu, G.; Helmerich, D. A.; Schubert, J.; Pearl, L. H.; Prodromou, C.; Neuweiler, H. Cooperation of Local Motions in the Hsp90 Molecular Chaperone ATPase Mechanism. *Nat. Chem. Biol.* **2016**, *12*, 628−635.
(31) Röhl, A.; Rohrberg, J.; Buchner, J. The Chaperone Hsp90: Changing Partners for Demanding Clients. *Trends Biochem. Sci.* **2013**, *38*, 253−262.
(32) Verba, K. A.; Wang, R. Y. R.; Arakawa, A.; Liu, Y.; Shirouzu, M.; Yokoyama, S.; Agard, D. A. Atomic Structure of Hsp90-Cdc37-Cdk4 Reveals That Hsp90 Traps and Stabilizes an Unfolded Kinase. *Science* **2016**, *352*, 1542−1547.
(33) Colombo, G.; Morra, G.; Meli, M.; Verkhivker, G. Understanding Ligand-Based Modulation of the Hsp90 Molecular Chaperone Dynamics at Atomic Resolution. *Proc. Natl. Acad. Sci. U. S. A.* **2008**, *105*, 7976−7981.
(34) Morra, G.; Verkhivker, G. G.; Colombo, G. Modeling Signal Propagation Mechanisms and Ligand-Based Conformational Dynamics of the Hsp90 Molecular Chaperone Full-Length Dimer. *PLoS Comput. Biol.* **2009**, *5*, e1000323.
(35) Verkhivker, G. M.; Dixit, A.; Morra, G.; Colombo, G. Structural and Computational Biology of the Molecular Chaperone Hsp90: From Understanding Molecular Mechanisms to Computer-Based Inhibitor Design. *Curr. Top. Med. Chem.* **2009**, *9*, 1369−1385.
(36) Morra, G.; Neves, M. A. C.; Plescia, C. J.; Tsustsumi, S.; Neckers, L.; Verkhivker, G.; Altieri, D. C.; Colombo, G. Dynamics-Based Discovery of Allosteric Inhibitors: Selection of New Ligands for the C-Terminal Domain of Hsp90. *J. Chem. Theory Comput.* **2010**, *6*, 2978−2989.
(37) Vettoretti, G.; Moroni, E.; Sattin, S.; Tao, J.; Agard, D. A.; Bernardi, A.; Colombo, G. Molecular Dynamics Simulations Reveal the Mechanisms of Allosteric Activation of Hsp90 by Designed Ligands. *Sci. Rep.* **2016**, *6*, 23830.
(38) Dixit, A.; Verkhivker, G. M. Probing Molecular Mechanisms of the Hsp90 Chaperone: Biophysical Modeling Identifies Key Regulators of Functional Dynamics. *PLoS One* **2012**, *7*, e37605.
(39) Morra, G.; Potestio, R.; Micheletti, C.; Colombo, G. Corresponding Functional Dynamics across the Hsp90 Chaperone Family: Insights from a Multiscale Analysis of MD Simulations. *PLoS Comput. Biol.* **2012**, *8*, e1002433.
(40) Seifert, C.; Gräter, F.; Dyson, H. J. Force Distribution Reveals Signal Transduction in E. Coli Hsp90. *Biophys. J.* **2012**, *103*, 2195−2202.
(41) Simunovic, M.; Voth, G. A. Molecular and Thermodynamic Insights into the Conformational Transitions of Hsp90. *Biophys. J.* **2012**, *103*, 284−292.
(42) Blacklock, K.; Verkhivker, G. M. Computational Modeling of Allosteric Regulation in the Hsp90 Chaperones: A Statistical Ensemble Analysis of Protein Structure Networks and Allosteric Communications. *PLoS Comput. Biol.* **2014**, *10*, e1003679.
(43) Blacklock, K.; Verkhivker, G. M. Differential Modulation of Functional Dynamics and Allosteric Interactions in the Hsp90-Cochaperone Complexes with p23 and Aha1: A Computational Study. *PLoS One* **2013**, *8*, e71936.
(44) Blacklock, K.; Verkhivker, G. M. Allosteric Regulation of the Hsp90 Dynamics and Stability by Client Recruiter Cochaperones: Protein Structure Network Modeling. *PLoS One* **2014**, *9*, e86547.
(45) Blacklock, K.; Verkhivker, G. M. Experimentally Guided Structural Modeling and Dynamics Analysis of Hsp90−p53 Inter-

DOI: 10.1021/acs.jcim.7b00630
J. Chem. Inf. Model. 2018, 58, 383−404

actions: Allosteric Regulation of the Hsp90 Chaperone by a Client Protein. *J. Chem. Inf. Model.* **2013**, *53*, 2962−2978.
(46) Johnson, J. L. Evolution and Function of Diverse Hsp90 Homologs and Cochaperone Proteins. *Biochim. Biophys. Acta, Mol. Cell Res.* **2012**, *1823*, 607−613.
(47) Šali, A. *MODELLER: A Program for Protein Structure Modeling*, Release 9.12, r9480; Rockefeller University, 2013; pp 779−815.
(48) Eisenberg, D.; Lüthy, R.; Bowie, J. U. VERIFY3D: Assessment of Protein Models with Three-Dimensional Profiles. *Methods Enzymol.* **1997**, *277*, 396−404.
(49) Colovos, C.; Yeates, T. O. Verification of Protein Structures: Patterns of Nonbonded Atomic Interactions. *Protein Sci.* **1993**, *2*, 1511−1519.
(50) Wiederstein, M.; Sippl, M. J. ProSA-Web: Interactive Web Service for the Recognition of Errors in Three-Dimensional Structures of Proteins. *Nucleic Acids Res.* **2007**, *35*, W407−W410.
(51) Li, J.; Sun, L.; Xu, C.; Yu, F.; Zhou, H.; Zhao, Y.; Zhang, J.; Cai, J.; Mao, C.; He, J.; et al. Structure Insights into Mechanisms of ATP Hydrolysis and the Activation of Human Heat-Shock Protein 90. *Acta Biochim. Biophys. Sin.* **2012**, *44*, 300−306.
(52) Obermann, W. M.; Sondermann, H.; Russo, A. A.; Pavletich, N. P.; Hartl, F. U. Vivo Function of Hsp90 Is Dependent on ATP Binding and ATP Hydrolysis. *J. Cell Biol.* **1998**, *143*, 901−910.
(53) Berendsen, H. J. C.; van der Spoel, D.; van Drunen, R. GROMACS: A Message-Passing Parallel Molecular Dynamics Implementation. *Comput. Phys. Commun.* **1995**, *91*, 43−56.
(54) MacKerell, A. D.; Bashford, D.; Bellott, M.; Dunbrack, R. L.; Evanseck, J. D.; Field, M. J.; Fischer, S.; Gao, J.; Guo, H.; Karplus, M.; et al. All-Atom Empirical Potential for Molecular Modeling and Dynamics Studies of Proteins. *J. Phys. Chem. B* **1998**, *102*, 3586−3616.
(55) Mackerell, A. D.; Feig, M.; Brooks, C. L. Extending the Treatment of Backbone Energetics in Protein Force Fields: Limitations of Gas-Phase Quantum Mechanics in Reproducing Protein Conformational Distributions in Molecular Dynamics Simulations. *J. Comput. Chem.* **2004**, *25*, 1400−1415.
(56) Best, R. B.; Zhu, X.; Shim, J.; Lopes, P. E. M.; Mittal, J.; Feig, M.; Mackerell, A. D., Jr. Optimization of the Additive CHARMM All-Atom Protein Force Field Targeting Improved Sampling of the Backbone Φ, ψ and Side-Chain χ(1) and χ(2) Dihedral Angles. *J. Chem. Theory Comput.* **2012**, *8*, 3257−3273.
(57) Brown, D. K.; Penkler, D. L.; Sheik Amamuddy, O.; Ross, C.; Atilgan, A. R.; Atilgan, C.; Tastan Bishop, Ö. MD-TASK: A Software Suite for Analyzing Molecular Dynamics Trajectories. *Bioinformatics* **2017**, *33*, 2768−2771.
(58) Atilgan, A. R.; Akan, P.; Baysal, C. Small-World Communication of Residues and Significance for Protein Dynamics. *Biophys. J.* **2004**, *86*, 85−91.
(59) Dijkstra, E. W. A Note on Two Problems in Connexion with Graphs. *Numer. Math.* **1959**, *1*, 269−271.
(60) Atilgan, C.; Atilgan, A. R. Perturbation-Response Scanning Reveals Ligand Entry-Exit Mechanisms of Ferric Binding Protein. *PLoS Comput. Biol.* **2009**, *5*, e1000544.
(61) Atilgan, C.; Gerek, Z. N.; Ozkan, S. B.; Atilgan, a. R. Manipulation of Conformational Change in Proteins by Single-Residue Perturbations. *Biophys. J.* **2010**, *99*, 933−943.
(62) Penkler, D.; Sensoy, Ö.; Atilgan, C.; Tastan Bishop, Ö. Perturbation-Response Scanning Reveals Key Residues for Allosteric Control in Hsp70. *J. Chem. Inf. Model.* **2017**, *57*, 1359−1374.
(63) Yilmaz, L. S.; Atilgan, A. R. Identifying the Adaptive Mechanism in Globular Proteins: Fluctuations in Densely Packed Regions Manipulate Flexible Parts. *J. Chem. Phys.* **2000**, *113*, 4454.
(64) Ikeguchi, M.; Ueno, J.; Sato, M.; Kidera, A. Protein Structural Change upon Ligand Binding: Linear Response Theory. *Phys. Rev. Lett.* **2005**, *94*, 78102.
(65) Atilgan, C.; Okan, O. B.; Atilgan, A. R. Network-Based Models as Tools Hinting at Nonevident Protein Functionality. *Annu. Rev. Biophys.* **2012**, *41*, 205−225.
(66) Okan, O. B.; Atilgan, A. R.; Atilgan, C. Nanosecond Motions in Proteins Impose Bounds on the Timescale Distributions of Local Dynamics. *Biophys. J.* **2009**, *97*, 2080−2088.
(67) Kabsch, W. A Solution for the Best Rotation to Relate Two Sets of Vectors. *Acta Crystallogr., Sect. A: Cryst. Phys., Diffr., Theor. Gen. Crystallogr.* **1976**, *32*, 922−923.
(68) Shen, M.; Sali, A. Statistical Potential for Assessment and Prediction of Protein Structures. *Protein Sci.* **2006**, *15*, 2507−2524.
(69) Eramian, D.; Eswar, N.; Shen, M.; Sali, A. How Well Can the Accuracy of Comparative Protein Structure Models Be Predicted? *Protein Sci.* **2008**, *17*, 1881−1893.
(70) Bowie, J. U.; Lüthy, R.; Eisenberg, D. A Method to Identify Protein Sequences That Fold into a Known Three-Dimensional Structure. *Science* **1991**, *253*, 164−170.
(71) Luethy, R.; Bowie, J. U.; Eisenberg, D. Assessment of Protein Models with Three-Dimensional Profiles. *Nature* **1992**, *356*, 83−85.
(72) Lobanov, M. Y.; Bogatyreva, N. S.; Galzitskaya, O. V. Radius of Gyration as an Indicator of Protein Structure Compactness. *Mol. Biol.* **2008**, *42*, 623−628.
(73) Flynn, J. M.; Mishra, P.; Bolon, D. N. A. Mechanistic Asymmetry in Hsp90 Dimers. *J. Mol. Biol.* **2015**, *427*, 2904−2911.
(74) Krukenberg, K. A.; Street, T. O.; Lavery, L. A.; Agard, D. A. Conformational Dynamics of the Molecular Chaperone Hsp90. *Q. Rev. Biophys.* **2011**, *44*, 229−255.
(75) Retzlaff, M.; Stahl, M.; Eberl, H. C.; Lagleder, S.; Beck, J.; Kessler, H.; Buchner, J. Hsp90 Is Regulated by a Switch Point in the C-Terminal Domain. *EMBO Rep.* **2009**, *10*, 1147−1153.
(76) Soroka, J.; Wandinger, S. K.; Mäusbacher, N.; Schreiber, T.; Richter, K.; Daub, H.; Buchner, J. Conformational Switching of the Molecular Chaperone Hsp90 via Regulated Phosphorylation. Mol. *Mol. Cell* **2012**, *45*, 517−528.
(77) Krukenberg, K. A.; Förster, F.; Rice, L. M.; Sali, A.; Agard, D. A. Multiple Conformations of E. Coli Hsp90 in Solution: Insights into the Conformational Dynamics of Hsp90. *Structure* **2008**, *16*, 755−765.
(78) Southworth, D. R.; Agard, D. A.; Burkholder, W. F.; Gragerov, A.; Ogata, C. M.; Gottesman, M. E.; Hendrickson, W. A.; Cagney, G.; Mai, D. Species-Dependent Ensembles of Conserved Conformational States Define the Hsp90 Chaperone ATPase Cycle. *Mol. Cell* **2008**, *32*, 631−640.
(79) Ozbaykal, G.; Rana Atilgan, A.; Atilgan, C. In Silico Mutational Studies of Hsp70 Disclose Sites with Distinct Functional Attributes. *Proteins: Struct., Funct., Genet.* **2015**, *83*, 2077−2090.
(80) Brown, D. K.; Sheik Amamuddy, O.; Tastan Bishop, Ö. Structure-Based Analysis of Single Nucleotide Variants in the Renin-Angiotensinogen Complex. *Glob. Heart* **2017**, *12*, 121−132.
(81) Dollins, D. E.; Immormino, R. M.; Gewirth, D. T. Structure of Unliganded GRP94, the Endoplasmic Reticulum Hsp90: Basis for Nucleotide Induced Conformational Change. *J. Biol. Chem.* **2005**, *280*, 30438−30447.
(82) Richter, K.; Reinstein, J.; Buchner, J. N-Terminal Residues Regulate the Catalytic Efficiency of the Hsp90 ATPase Cycle. *J. Biol. Chem.* **2002**, *277*, 44905−44910.
(83) Lavery, L. A.; Partridge, J. R.; Ramelot, T. A.; Elnatan, D.; Kennedy, M. A.; Agard, D. A. Structural Asymmetry in the Closed State of Mitochondrial Hsp90 (TRAP1) Supports a Two-Step ATP Hydrolysis Mechanism. *Mol. Cell* **2014**, *53*, 330−343.
(84) Prodromou, C.; Panaretou, B.; Chohan, S.; Siligardi, G.; O'Brien, R.; Ladbury, J. E.; Roe, S. M.; Piper, P. W.; Pearl, L. H. The ATPase Cycle of Hsp90 Drives a Molecular "Clamp" via Transient Dimerization of the N-Terminal Domains. *EMBO J.* **2000**, *19*, 4383−4392.
(85) Liu, R.; Hu, J.; Thornton, J.; Singh, M.; Funkhouser, T. Computational Prediction of Heme-Binding Residues by Exploiting Residue Interaction Network. *PLoS One* **2011**, *6*, e25560.
(86) del Sol, A.; Fujihashi, H.; O'Meara, P. Topology of Small-World Networks of Protein-Protein Complex Structures. *Bioinformatics* **2005**, *21*, 1311−1315.
(87) Cheng, T. M.-K.; Blundell, T. L.; Fernandez-Recio, J. pyDock: Electrostatics and Desolvation for Effective Scoring of Rigid-Body

DOI: 10.1021/acs.jcim.7b00630
J. Chem. Inf. Model. 2018, 58, 383−404

Protein-Protein Docking. *Proteins: Struct., Funct., Genet.* **2007**, *68*, 503−515.
(88) Taylor, N. R. Small World Network Strategies for Studying Protein Structures and Binding. *Comput. Struct. Biotechnol. J.* **2013**, *5*, e201302006.
(89) Mollapour, M.; Tsutsumi, S.; Truman, A. W.; Xu, W.; Vaughan, C. K.; Beebe, K.; Konstantinova, A.; Vourganti, S.; Panaretou, B.; Neckers, L.; et al. Threonine 22 Phosphorylation Attenuates Hsp90 Interaction with Cochaperones and Affects Its Chaperone Activity. *Mol. Cell* **2011**, *41*, 672−681.
(90) Cunningham, C. N.; Krukenberg, K. A.; Agard, D. A. Intra- and Intermonomer Interactions Are Required to Synergistically Facilitate ATP Hydrolysis in Hsp90. *J. Biol. Chem.* **2008**, *283*, 21170−21178.
(91) Neckers, L. Hsp90 Inhibitors as Novel Cancer Chemotherapeutic Agents. *Trends Mol. Med.* **2002**, *8*, S55−61.
(92) Hessling, M.; Richter, K.; Buchner, J. Dissection of the ATP-Induced Conformational Cycle of the Molecular Chaperone Hsp90. *Nat. Struct. Mol. Biol.* **2009**, *16*, 287−293.
(93) Xu, W.; Mollapour, M.; Prodromou, C.; Wang, S.; Scroggins, B.; Palchick, Z.; Beebe, K.; Siderius, M.; Lee, M.-J.; Neckers, L.; et al. Dynamic Tyrosine Phosphorylation Modulates Cycling of the HSP90-P50CDC37-AHA1 Chaperone Machine. *Mol. Cell* **2012**, *47*, 434−443.
(94) Siligardi, G.; Hu, B.; Panaretou, B.; Piper, P. W.; Pearl, L. H.; Prodromou, C. Co-Chaperone Regulation of Conformational Switching in the Hsp90 ATPase Cycle. *J. Biol. Chem.* **2004**, *279*, 51989−51998.
(95) Rehn, A.; Moroni, E.; Zierer, B. K.; Tippel, F.; Morra, G.; John, C.; Richter, K.; Colombo, G.; Buchner, J. Allosteric Regulation Points Control the Conformational Dynamics of the Molecular Chaperone Hsp90. *J. Mol. Biol.* **2016**, *428*, 4559−4571.
(96) Panaretou, B.; Siligardi, G.; Meyer, P.; Maloney, A.; Sullivan, J. K.; Singh, S.; Millson, S. H.; Clarke, P. A.; Naaby-Hansen, S.; Prodromou, C.; et al. Activation of the ATPase Activity of hsp90 by the Stress-Regulated Cochaperone aha1. *Mol. Cell* **2002**, *10*, 1307−1318.
(97) Street, T. O.; Zeng, X.; Pellarin, R.; Bonomi, M.; Sali, A.; Kelly, M. J. S.; Chu, F.; Agard, D. A. Elucidating the Mechanism of Substrate Recognition by the Bacterial Hsp90 Molecular Chaperone. *J. Mol. Biol.* **2014**, *426*, 2393−2404.
(98) Genest, O.; Reidy, M.; Street, T. O.; Hoskins, J. R.; Camberg, J. L.; Agard, D. A.; Masison, D. C.; Wickner, S. Uncovering a Region of Heat Shock Protein 90 Important for Client Binding in E. Coli and Chaperone Function in Yeast. *Mol. Cell* **2013**, *49*, 464−473.
(99) General, I. J.; Liu, Y.; Blackburn, M. E.; Mao, W.; Gierasch, L. M.; Bahar, I. ATPase Subdomain IA Is a Mediator of Interdomain Allostery in Hsp70 Molecular Chaperones. *PLoS Comput. Biol.* **2014**, *10*, e1003624.
(100) Abdizadeh, H.; Guven, G.; Atilgan, A. R.; Atilgan, C. Perturbation Response Scanning Specifies Key Regions in Subtilisin Serine Protease for Both Function and Stability. *J. Enzyme Inhib. Med. Chem.* **2015**, *30*, 867.
(101) Abdizadeh, H.; Atilgan, C. Predicting Long Term Cooperativity and Specific Modulators of Receptor Interactions in Human Transferrin from Dynamics within a Single Microstate. *Phys. Chem. Chem. Phys.* **2016**, *18*, 7916−7926.
(102) Meyer, P.; Prodromou, C.; Liao, C.; Hu, B.; Roe, S. M.; Vaughan, C. K.; Vlasic, I.; Panaretou, B.; Piper, P. W.; Pearl, L. H. Structural Basis for Recruitment of the ATPase Activator Aha1 to the Hsp90 Chaperone Machinery. *EMBO J.* **2004**, *23*, 1402−1410.
(103) Panaretou, B. ATP Binding and Hydrolysis Are Essential to the Function of the Hsp90 Molecular Chaperone Invivo. *EMBO J.* **1998**, *17*, 4829−4836.
(104) Retzlaff, M.; Hagn, F.; Mitschke, L.; Hessling, M.; Gugel, F.; Kessler, H.; Richter, K.; Buchner, J. Asymmetric Activation of the hsp90 Dimer by Its Cochaperone aha1. *Mol. Cell* **2010**, *37*, 344−354.
(105) Sattin, S.; Tao, J.; Vettoretti, G.; Moroni, E.; Pennati, M.; Lopergolo, A.; Morelli, L.; Bugatti, A.; Zuehlke, A.; Colombo, G. Activation of Hsp90 Enzymatic Activity and Conformational Dynamics through Rationally Designed Allosteric Ligands. *Chem. - Eur. J.* **2015**, *21*, 13598−13608.
(106) Schmid, A. B.; Lagleder, S.; Gräwert, M. A.; Röhl, A.; Hagn, F.; Wandinger, S. K.; Cox, M. B.; Demmer, O.; Richter, K.; Buchner, J.; et al. The Architecture of Functional Modules in the Hsp90 Co-Chaperone Sti1/Hop. *EMBO J.* **2012**, *31*, 1506−1517.
(107) Hatherley, R.; Blatch, G. L.; Bishop, O. T. Plasmodium Falciparum Hsp70-X: A Heat Shock Protein at the Host-Parasite Interface. *J. Biomol. Struct. Dyn.* **2014**, *32*, 1766−1779.
(108) Buchner, J.; Li, J. Structure, Function and Regulation of the hsp90 Machinery. *Biomed. J.* **2013**, *36*, 106−117.
(109) Verkhivker, G. M. Computational Studies of Allosteric Regulation in the Hsp90 Molecular Chaperone: From Functional Dynamics and Protein Structure Networks to Allosteric Communications and Targeted Anti-Cancer Modulators. *Isr. J. Chem.* **2014**, *54*, 1052−1064.

DOI: 10.1021/acs.jcim.7b00630
J. Chem. Inf. Model. 2018, 58, 383−404